Energy spectra, angular spread and dose distributions of electron beams from various accelerators used in radiotherapy

PIRS-0439

G.X. Ding and D.W.O. Rogers
Institute for National Measurement Standards
Ottawa, Canada K1A 0R6
TEL: (613) 993-2715
FAX: (613) 952-9865

E-mail: gding@irs.phy.nrc.ca
or
E-mail: dave@irs.phy.nrc.ca (drogers at physics.carleton.ca since Dec 2003)

April, 1995

Contents

List of Tables

List of Figures

1 Introduction

The energy and angular distributions of electrons and contaminant photons from medical accelerator are the most important characteristics of a radiotherapy electron beam. A knowledge of clinical beams is essential for dosimetry, treatment planning, quality assurance, and design of an accelerator. In the radiation treatment of cancer the treatment plan can only be made correctly if characteristics of the beam are known. Beam quality has influence on the physical, chemical and radiobiological effects as well as on the response of various detectors. Due to the variations of an applicator's design the properties of scattered electrons are complicated[1, 2] and these scattered electrons may have a large influence on the dose distributions in a patient. Experimentally it is difficult to obtain detailed information because of various limitations in the clinical environment and detectors[3]. In addition to this, it is virtually impossible using experimental methods to distinguish electrons which are scattered from the beam defining system.

The EGS4 Monte Carlo simulation code, BEAM, is a powerful and flexible tool to simulate realistic clinical radiation beams and to obtain a detailed knowledge of the characteristics of therapy beams from accelerators. A previous study[1] described the code and simulation in detail and demonstrated that BEAM can predict dose distributions very accurately. Here we will systematically analyze the simulated beams from a variety of electron accelerators including the NRCC research accelerator, the University of Wisconsin Varian Clinac 2100C, a Philips SL75-20, the Ottawa Regional Cancer Center Siemens KD2 and AECL Therac 20 and the Memorial Sloan-Kettering Cancer Center Scanditronix Racetrack MM50. These accelerators have very different designs and some of them produce scanned beams instead of scattered beams. The energy range of electron beams is from 5 to 50 MeV. Figures 1 to 8 are the representations of six of the accelerator's treatment head studied in this work as shown by EGS_windows[4]. The figures show the actual simulation of particles transported inside the treatment head.

For beams produced by various accelerators this report contains detailed information on the energy and angular distribution of: all electrons; scattered electrons from each beam defining component; and contaminant photons. Comparisons between calculated and mea-

sured dose distributions in water phantoms are presented along with calculated dose components contributed by contaminant photons and electrons scattered from beam defining components.

It must be emphasized that results apply to the specific accelerators studied and should not be taken as applying to all similar machines (e.g. the Univ. of Wisconsin Clinac 2100C had special foils to match beams with an earlier Clinac 1800).

2 Monte Carlo Calculation

The EGS4 user code BEAM[1] is used to simulate accelerators and obtain detailed information about each particle emerging from an accelerator. The position, energy, angle and a complete history of where a particle has been are stored in a "phase-space" data file. The phase-space data files are used repeatedly for analyzing beam or as input to the EGS4 user code DOSXYZ[5] to calculate the dose distributions in a water phantom.

By using the variable LATCH[1] which records each particle's complete history in the beam simulation we are able to obtain not only the energy spectra of all electrons and contaminant photons but also the spectra of electrons and photons scattered from collimators or applicators of the beam defining system.

The DOSXYZ code has been modified to read a phase-space file produced by the BEAM simulation as an incident beam and to make use of the variable LATCH to calculate dose components contributed by scattered electrons and contaminant photons in the beam.

The beam field size studied here is 10×10 cm^2 for beams with energies below 22 MeV and 25×25 cm^2 or 20×20 cm^2 for those with energies above 22 MeV. The SSD is 100 cm and 110 cm for energies 5 – 40 MeV and 50 MeV, respectively. The monoenergetic electron energies at the exit vacuum window are adjusted to match R_{50}, the depth at which the dose falls to 50% of dose maximum on the measured central-axis depth-dose curve in a water phantom.

The spectra presented in the following are for incident monoenergetic beams and any width in the incident beam energy spectrum at the exit vacuum window of an accelerator

would add to the breadth of the final spectra [6].

In the beam simulation the energy cutoffs for particle transport are set to ECUT = 0.700 MeV, AE = 0.521 MeV (total energy) and PCUT = AP = 0.010 MeV to ensure adequate energy-loss straggling. In the dose calculations the energy cutoffs for particle transport are set to ECUT = AE = 0.700 MeV (total energy) and PCUT = AP = 0.010 MeV. In all cases, the PRESTA electron transport algorithm[7] is employed with ESTEPE = 0.01 or 0.04.

3 Results and Discussion

3.1 Overview and statistics of the results

There are about 10^6 electrons inside the beam field in the phase-space file of a simulated beam. Since a phase-space file contains particles outside the beam field as well as contaminant photons, the actual number of particles in a phase-space file varies depending on the characteristics of the beam.

The two computer codes, PHSP_EXY and PHSP_SPECXY[8], are used to analyze the phase-space files from BEAM to obtain the mean energy and energy spectra of simulated beams at the surface of the phantom. The codes allow the user to select particles according to particle's history by making use of the LATCH feature of BEAM[1].

The spectra and angular distributions of electrons as well as photons presented in the following figures are all normalized to 1 for the peak of electron spectra. The bin size of spectra and angular distributions is 100 keV and 1° for all beams. The angle θ is relative to the z-axis which is the central-axis of the beam. The figure captions each specify how many electrons are in the bins normalized to 1 for energy and angular distributions. One can thereby determine n, the number of electrons in each bin, and hence the fractional statistical uncertainty which is given by $\sqrt{n}/n$ (1 standard deviation).

The dose distributions are all normalized to 100% for the maximum of the total dose which is contributed by all electrons and contaminant photons in the beam. The statistical uncertainties on the depth-dose cuvers are typically 1% or better.

Table 1 summarizes characteristics of simulated clinical electron beams from five accelerators. The average kinetic energies $\overline{\mathrm{E}}$ refer to the number averaged inside the irradiated field at the phantom surface. $\mathrm{E_p}$ is the most probable energy inside the field at the surface of the phantom. Direct electrons are those which do not include electrons scattered from the beam defining system of a treatment head. The difference in surface doses between total and that from direct electrons is indicative of the number and angle of scattered electrons in the beam. $\mathrm{R_{50}}$ and $\mathrm{R_p}$ are obtained from calculated central-axis depth-dose curves. The % surface doses of total (contributed by all particles in the simulated beam) or direct (contributed only by those electrons that do not hit any jaws, collimators or applicators) is relative to maximum total dose. E_{max} for electrons and photons is the maximum energy of electrons (kinetic energy) and photons in the phase-space file respectively. The difference between the maximum electron and contaminant photon energy reflects the total thickness of vacuum exit window, scattering foils, beam monitor chamber, mirror and air in the beam. The maximum contaminant photon energy is about the kinetic energy of the incident electron at the exit vacuum window.

Table 2 presents the simulation data of clinical electron beams from five medical accelerators. E_{in} is the incident electron kinetic energy at the exit vacuum window of an accelerator. It is adjusted to match the calculated $\mathrm{R_{50}}$ to that of the measurement. $\mathrm{e^-}/100$ inc $\mathrm{e^-}$ and $\gamma/100$ inc $\mathrm{e^-}$ inside field are the number of electrons and number of photons inside the field per 100 incident electrons at the exit vacuum window. These data can be used to estimate the number of incident electrons (at the exit vacuum window) that the simulation has to run to produce the required number of electrons at the phantom surface and inside the beam field. % direct $\mathrm{e^-}$ and % direct $\mathrm{e^-}$ are defined as:

$$\%\ direct\ e^- = \frac{number\ of\ direct\ electrons\ inside\ field}{number\ of\ total\ electrons\ inside\ field} \tag{1}$$

$$\%\ direct\ \gamma = \frac{number\ of\ direct\ photons\ inside\ field}{number\ of\ total\ photons\ inside\ field} \tag{2}$$

where direct electrons or photons are those that do not hit any jaws, collimators or applicators. The cpu per incident history is machine dependent as well as simulation parameter dependent[1]. The data presented in table 2 are for an SGI Indigo with an R4400 cpu.

It is interesting to note that there is almost no build-up in the component of the central-

axis depth-dose curves contributed by electrons scattered from applicators. This is due to the combination of the broad angular distributions and the low-energy spectra of electrons from applicators.

3.2 Electron beams from the NRCC research accelerator

The NRCC accelerator is a Vickers research accelerator with no head assembly. The geometry of the experimental set up (fig.1) includes a titanium exit vacuum window (0.127 mm thick), a tungsten scattering foil (0.092 mm thick), a square collimator (steel, 20.3 cm thick) and a monitoring ion chamber (very thin mylar). The water phantom container is made of PMMA (9 mm thick). The beams irradiate the water phantom horizontally. The field size is 8×8 cm^2 on the phantom surface and SSD = 96 cm. The energy of the electron beam exiting the vacuum window is known independently with an accuracy of $\pm1\%$[9]. The two beams (10.0 and 20.0 MeV) have an identical experimental set up except for the incident electron energy at the exit vacuum window. The dose measurements have been done with a small diode detector, a parallel plate ion chamber and a cylindrical farmer chamber. After correction of the ion chamber results for stopping power ratios, all three measurement techniques gave the same results within 0.5%. The measured data are from Carl Ross of National Research Council of Canada.

The results for these two beams are shown in figure 9 and 10 respectively. Because of the geometry of the experimental set up, the electron's energy spread is very small and there are few contaminant photons in the beams. The two beams have narrow angular spread although the electrons from the jaws lead to a small tail right out to 80°. Note that in order to match the experimental values of R_{50} in the central-axis depth-dose curves the incident electron energies at the exit vacuum window used in the simulation were increased by 1.5% compared to those determined independently (*viz.* 10 and 20 MeV). This slight discrepancy may be caused by the measured energy or by the stopping power used in the calculation (to be resolved in future investigations). The remarkable agreement between calculated and measured dose distributions shown in fig.10 marked a milestone in benchmarking the simulation code BEAM[10].

3.3 Electron beams from a Varian Clinac 2100C accelerator

The Varian Clinac 2100C accelerator (fig.2) has an exit window, scattering foils, a beam monitor ion chamber, a mirror, a "shielding plate", X and Y jaws and an electron applicator. This particular accelerator at the Wisconsin Comprehensive Cancer Center in Madison has thicker scattering foils (same as in an older Clinac 1800) in order to match the depth-dose curves of an earlier machine. It also has the relatively thick-walled gold-plated mica ion chamber and a type II applicator cone with 4 relatively thin scrapers[1]. All measured data are from Carol Wells and Rock Mackie of the University of Wisconsin.

Figures 11, 12, 13, 14 and 15 present the spectra and the angular distributions at the phantom surface and comparison between calculated and measured dose distributions along with dose components contributed from each beam defining component from 6, 9, 12, 15 and 18 MeV electron beams respectively.

There is excellent agreement between calculations and measurements. All dose measurements have been done with a small diode detector.

Note that there are two peaks in the electron spectra for all beams. The low-energy peak is caused by electrons passing through a 6 mm aluminum applicator scraper and remaining in the beam[1] based on a detailed study which separated the spectra from each scraper component.

Note that the total bremsstrahlung tails in the depth-dose curves are contributed mainly by the contaminant photons in the beams.

In order to explain experimental observations[11] on the influence of an applicator design we also simulate the 9 MeV beam with a newer applicator design (Type III). The energy and angular distributions with this new applicator cone (Type III) from a 9 MeV beam are shown in figure 16 which should be compared to figure 12 for the Type II applicator. The scattered electrons from the applicator are greatly reduced and the second low-energy peak disappears. The surface dose contributed by scattered electrons from the applicator is reduced from 17% with Type II applicator to 8% with the Type III applicator.

By calculation it was found that the peak could be made to disappear using an additional

piece of lead on the top of this part of the applicator. Figure 17 presents the result of a 9 MeV beam with our modified applicator design. The calculated depth-dose curve with the lead in place was virtually identical to that of the new design applicator shown in figures 16 and 17 respectively. The calculated dose profiles at d_{max} for these three different applicators along with dose components are shown in figure 18. After this "discovery", we learned that Varian sells an upgrade kit which has a similar design and performs the same function.

3.4 Electron beams from a Philips SL75-20 accelerator

The geometry of the SL75-20 accelerator shown in fig.5 can be found in references[12, 13, 14]. It has an exit window, primary collimator, scattering foils (there are three scattering foil positions in a carousel in the treatment head, the appropriate one is set according the beam energy), a beam monitor ion chamber, a steel shielding ring, a mirror, X and Y jaws, an accessory ring and electron applicators which are solid-walled flat tubes made of aluminium. The measured data are from Udale-Smith, reference [13].

Our results for the electron spectrum from the 5 MeV beam are similar to those of earlier study by Udale-Smith[14] although there are some unexplained differences[1].

Figures 19, 20, 21, 22 and 23 present the energy spectra and angular distributions of electrons and contaminant photons and dose distributions along with dose components contributed from each beam defining component for 5, 10, 14, 17 and 20 MeV electron beams respectively. Good agreement is obtained between calculated and measured central-axis depth-dose curves. Calculated dose profiles at the phantom surface and at d_{max} (1.1 cm depth) are shown in figure 24 for the 5 MeV beam. It can be seen that even at d_{max}, dose contributions from scattered electrons are significant (33%).

The electron spectra from the SL75-20 have a wide spread partially because of its thicker scattering foils.

At higher beam energies there are two small peaks in the energy spectra. This is due to the geometry of the scattering foils which are stacked cylinders with increasing radii (see fig. 25). Electrons going through the scattering foils near the central-axis lose more energy. A simulation, which uses LATCH to separate components which have passed through various

thickness of scattering foils, is shown in figure 25.

Again due to the design of the applicator of the SL75-20 there is a considerable amount of dose contribution from scattered electrons, particularly from the applicator (about 32% to 22% of total surface dose for 5 to 20 MeV beams respectively).

3.5 Electron beams from a Siemens KD2 accelerator

The geometry of the Siemens KD2 accelerator shown in fig.6 consists of an exit vacuum window, primary collimator, scattering foils, a beam monitor ion chamber, a mirror, x and y jaws, and electron applicators which are solid-walled flat tubes made of aluminium with scrapers of brass, steel and aluminium. The experimental data are from Joanna Cygler of Ottawa Regional Cencer Center (6 and 11 MeV) and from Jack Janssen and Henk Huizenga of the Dr Daniel den Hoed Cancer Clinic Netherlands (21 MeV beam). We have also tried to simulate other beams with higher energies from the Ottawa clinics KD2 but we are unable to reproduce the measured high bremsstrahlung tail. This may be due to our lack of an accurate description of the scattering foils of the accelerator for these higher energies.

Figures 26, 27 and 28 show the energy spectra and angular distributions of electrons and contaminant photons and dose distributions along with dose components contributed from each beam defining component for 6, 11 and 21 MeV electron beams respectively.

The dose measurements (6 and 11 MeV beam) have been done with a small diode detector. The 21 MeV beam data have been measured with an NACP plane parallel ionization chamber, using the NACP protocol to convert ionization to dose.

Excellent agreement is obtained between calculated and measured central-axis depth-dose curves for these beam energies except for the photon tail of the 21 MeV beam which is underestimated.

Figure 29 presents calculated dose profiles at the phantom surface and at d_{max} from various components of an 11 MeV beam from the KD2 accelerator.

Due to the applicator design of the KD2 there are more scattered electrons near the field boundary than near the central-axis. The dose profiles contributed by electrons scattered

from the applicator become flatter at larger depth because scattered electrons from the applicator have lower energy and relatively large angle.

3.6 Electron beams from an AECL Therac 20 accelerator

The Therac 20 accelerator shown in fig.7 uses a scanned beam to achieve a flat beam profile. There are no scattering foils in this accelerator. The geometry consists of an exit vacuum window, a beam monitor ion chamber, a series of x and y jaws and electron beam applicators. The beam monitor chamber is made with aluminized Kapton and the applicator has thick scraper bars. For the Therac 20 the scan pattern (see reference [1]) was set for a 40×40 cm^2 field but the treatment field was 10×10 cm^2.

The experimental data have been measured with a diode detector by Joanna Cygler of the Ottawa Regional Cancer Center.

Figures 30, 32, 33, 34 and 35 show the energy spectra and angular distributions of electrons and contaminant photons and comparison between calculated and measured central-axis depth-dose curves along with dose components contributed from each beam defining component for 6, 9, 13, 17 and 20 MeV beams respectively.

Due to the combination of no scattering foils and the design of the beam defining system, particularly the design of the applicator in the Therac 20, both the energy and angular spread of the electrons are small.

There are few contaminant photons in the beam. The large angular spread of contaminant photons is due to the fact that most contaminant photons are originated from the beam defining system.

Figure 31 presents a comparison of calculated and measured dose profiles at the depth of d_{max} and at the phantom surface from various dose components for a 6 MeV beam from the AECL Therac 20. The agreement is excellent.

3.7 Electron beams from a Racetrack MM50 accelerator

The geometry of the Scanditronix MM50 (see fig.8) at the Memorial Sloan Kettering Cancer Center consists of an exit vacuum window, a thin scattering foil, a beam monitor ion chamber, a mirror, a primary collimator and a multileaf collimator which is set to a square for these calculations. The accelerator head is filled with helium gas. The MM50 uses both beam scanning and a very thin scattering foil to give a uniform beam distribution. The beam sizes simulated are larger than for the lower-energy beams from other accelerators to ensure broad-beam conditions. Unlike other accelerators, this machine does not have electron applicators at these beam energies. The beam is shaped by the primary collimator and the multileaf collimator. The scan pattern was set for a circle of 18 cm radius according to the machine specifications.

Figures 36, 37 and 38 show the energy spectra of 25, 40 and 50 MeV beams incident on the phantom surface and inside the treatment field.

The energy spectra from this accelerator are very narrow and close to monoenergetic because of two factors: the scanned beam and the large air space between last part of the beam defining system and the phantom surface. This air gap means many of the electrons scattered from the beam defining system leave the field.

Note that in the central-axis depth-dose curves the contaminant photons in the beam have a negligible contribution to the bremsstrahlung tails.

Figure 39 presents calculated dose profiles at various depths in a water phantom for the 25 MeV and the 50 MeV beams from the Scanditronix Medical Microtron 50. The beams are very flat across the field at various depths in a water phantom.

4 Conclusion

We have presented energy and angular distributions, as well as dose components of clinical electron beams from various medical accelerators with energy ranging from 5 to 50 MeV along with a detailed study of spectra of scattered electrons from the beam defining components.

The spectra presented here are based on simulated clinical beams. We have calculated dose distributions using the simulated beams. The calculated and measured dose distributions in water phantoms are in very good agreement in all cases which give us the confidence that the simulations are accurate.

This investigation demonstrates the strength of the full Monte Carlo simulation of accelerator head which allow us to obtain detailed information of clinical electron beams. This information enhances our knowledge on many aspects of clinical electron beams. Extensive beam data from various medical accelerators presented here will be very useful in understanding the characteristics of the clinical electron beams. The information obtained from the simulation is critical to many aspects of optimal radiotherapy and will help to make more accurate treatment planning and improve electron beam dosimetry. The simulated realistic clinical beam can be used to calculate various dosimetry parameters [8, 6, 15] and to reduce the uncertainty of these parameters which have been calculated using monoenergetic beams because of lack of details of realistic beams.

This report and data sets for all figures are available on the www (word-wide-web) at http://www.physics.carleton.ca/∼drogers/pubs/papers .

5 Acknowledgements

This work is part of the overall development of the BEAM code and we thank our collaborators, Drs Charlie Ma and Bruce Faddegon at NRC and Rock Mackie at University of Wisconsin for their work to make this code work so well. We wish to thank following individuals for providing the data related to various accelerator beams: Dr. Carl Ross for data related to the NRC accelerator, Carol Wells and Rock Mackie of the University of Wisconsin for data related to the Clinac 2100C, Cal Huntzinger of Varian for supplying detailed information on the Clinac 2100, Dr. Joanna Cygler of Ottawa Regional Cancer Center for data related to the KD2 and the Therac 20, Mr. Mark McCarthy of Siemens for supplying information on the KD2, Drs. Jack Janssen and Henk Huizenga of the Dr Daniel den Hoed Cancer Clinic for data related to the Siemens KD2, and Dr. Chen Chui of Memorial Sloan-Kettering Cancer Center in New York for the data related to the Racetrack Microtron. We

thank Dr. Alex Bielajew for supporting the EGS4 system at NRC and his help running EGS_Windows and Dr Michel Proulx for work on the computing systems. This work is partially supported by NCI grant R01CA52692. George Ding is the recipient of the MRC Studentships Award and is grateful to the Medical Research Council of Canada.

Table 1: Characteristics of simulated clinical electron beams from 5 clinical electron accelerators. The energies are all number averaged values for particles inside the beam and above 189 keV kinetic energy fro e^- and 10 keV for photons. E_{max} is the maximum kinetic energy for particles anywhere in the scoring plane (at the surface of the phantom here).

Linac	beam energy MeV	R_{50} cm	R_p cm	E_p MeV	% surface dose total $e^-+\gamma$	% surface dose direct e^-	$\overline{E}$ MeV e^-	$\overline{E}$ MeV γ	E_{max} MeV e^-	E_{max} MeV γ
	6	2.63	3.26	6.88	82	61	6.11	1.36	7.10	7.94
Clinac	9	4.00	5.03	10.39	85	60	9.10	1.85	10.59	11.66
2100C	12	5.18	6.30	13.05	89	70	11.74	2.19	13.23	14.33
	15	6.50	7.92	16.31	92	70	14.59	2.52	16.62	17.52
	18	7.72	9.45	19.49	93	70	17.35	2.81	19.67	20.73
	5	2.08	2.60	5.66	78	47	5.07	1.23	5.90	6.68
SL75	10	4.12	5.20	10.66	88	55	9.34	1.96	10.98	11.98
-20	14	5.98	7.40	15.34	93	57	13.28	2.52	15.82	16.79
	17	6.96	8.70	17.79	93	61	15.28	2.98	18.67	19.68
	20	8.10	10.0	21.04	94	61	17.76	3.35	21.96	22.96
	6	2.31	2.84	6.05	73	62	5.53	1.30	6.17	6.99
KD2	11	4.21	5.12	10.51	81	70	9.70	1.88	10.63	11.45
	21	8.30	10.1	20.59	89	79	18.74	3.11	20.78	21.87
	6	2.18	2.68	5.60	68	65	5.50	1.00	5.62	5.86
Therac	9	3.42	4.12	8.42	74	70	8.25	1.30	8.43	8.65
20	13	5.14	6.15	12.41	80	76	12.14	1.66	12.42	12.53
	17	6.85	8.10	16.35	88	82	15.93	1.97	16.35	16.57
	20	8.10	9.63	19.30	90	85	18.74	2.17	19.31	19.47
	25	10.36	12.30	24.77	92	92	24.53	3.50	24.78	24.81
MM50	40	15.47	19.50	39.50	94	94	38.90	4.91	39.50	39.60
	50	18.55	24.00	49.69	95	95	48.90	5.59	49.69	49.73

Table 2: Simulation data of clinical electron beams from five medical accelerators. The field size is 10×10 cm^2 except beams from MM50 where field sizes are 25×25 (25 and 40 MeV beams) and 20×20 (50 MeV beam). The cpu time is for an R4400 cpu in an SGI Indigo.

Machine	beam nominal energy	E_{in} incident MeV	e^- in field /10^2 inc e^-	γ in field /10^2 inc e^-	% direct e^-	% direct γ	cpu /inc e^- ms
Clinac 2100C	6	8.00	2.15	2.10	78.9	69.6	24.1
	9	11.70	2.99	4.15	74.8	67.4	44.8
	12	14.35	3.83	5.83	82.9	70.9	56.3
	15	17.62	5.59	9.08	81.5	67.2	45.7
	18	20.80	7.48	12.7	80.8	63.7	74.2
SL75-20	5	6.70	2.06	1.21	65.2	71.4	9.78
	10	12.00	4.14	4.05	66.8	75.6	13.2
	14	16.80	11.8	13.4	66.4	72.1	29.4
	17	19.70	5.59	10.1	70.0	80.1	18.8
	20	23.00	6.95	13.6	69.5	78.5	54.4
KD2	6	7.00	0.70	1.10	84.5	79.9	9.07
	11	11.55	2.72	3.18	87.2	77.0	11.1
	21	21.88	5.59	11.7	90.0	70.7	18.0
Therac 20	6	5.88	3.68	0.52	96.1	25.1	62.2
	9	8.69	5.60	1.35	95.9	16.3	92.0
	13	12.69	6.09	2.58	95.6	10.5	125.
	17	16.63	6.25	3.93	95.3	7.42	165.
	20	19.59	6.33	5.07	94.8	5.98	197.
MM50	25	24.90	84.9	4.97	99.6	50.9	46.7
	40	39.65	82.1	11.4	99.4	58.6	82.2
	50	49.86	51.0	10.6	99.1	42.0	155.

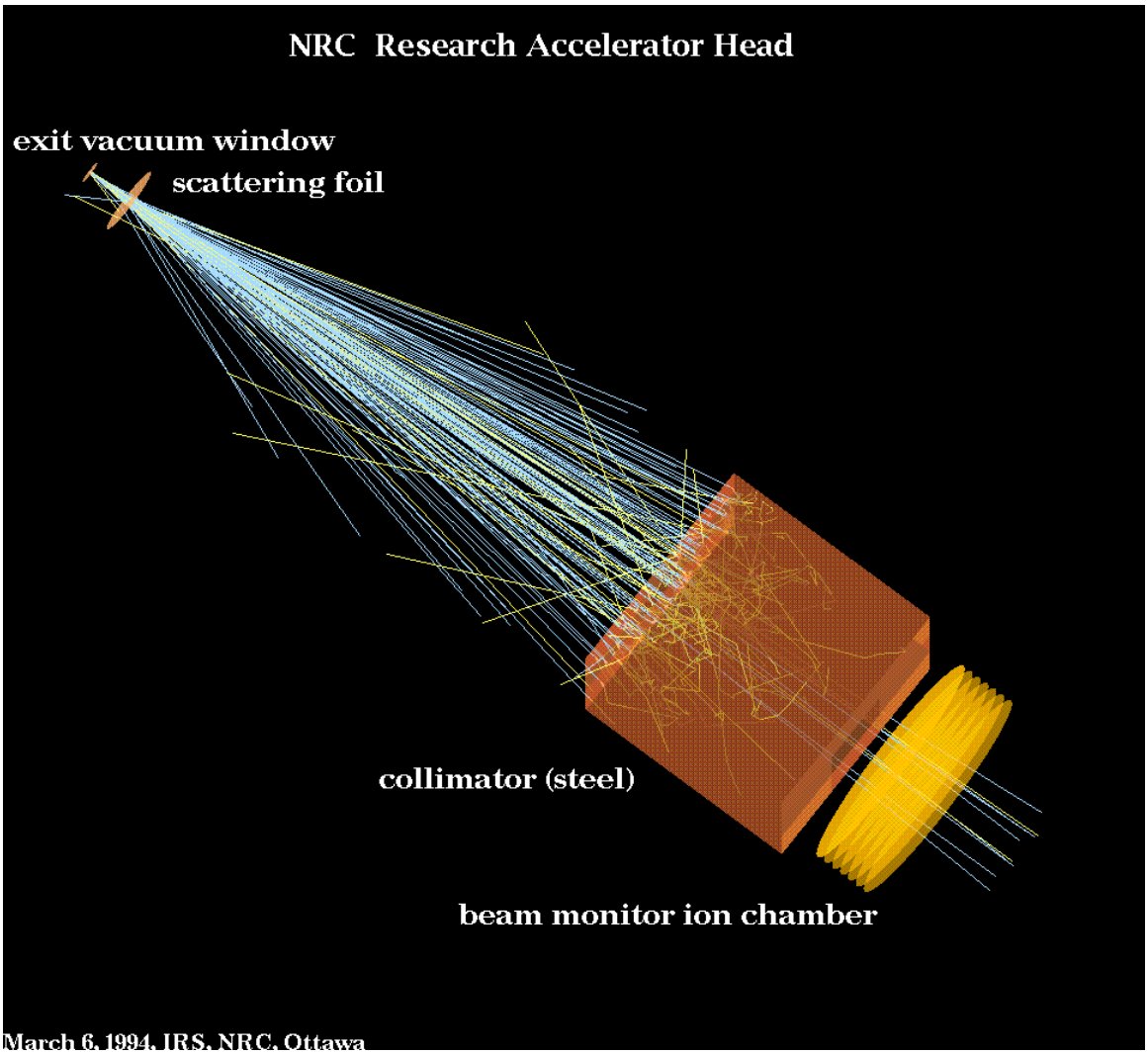

Figure 1: A 20 MeV electron beam from the NRC research accelerator as shown by EGS_windows with about 100 histories. See section 3.2 for a detailed description.

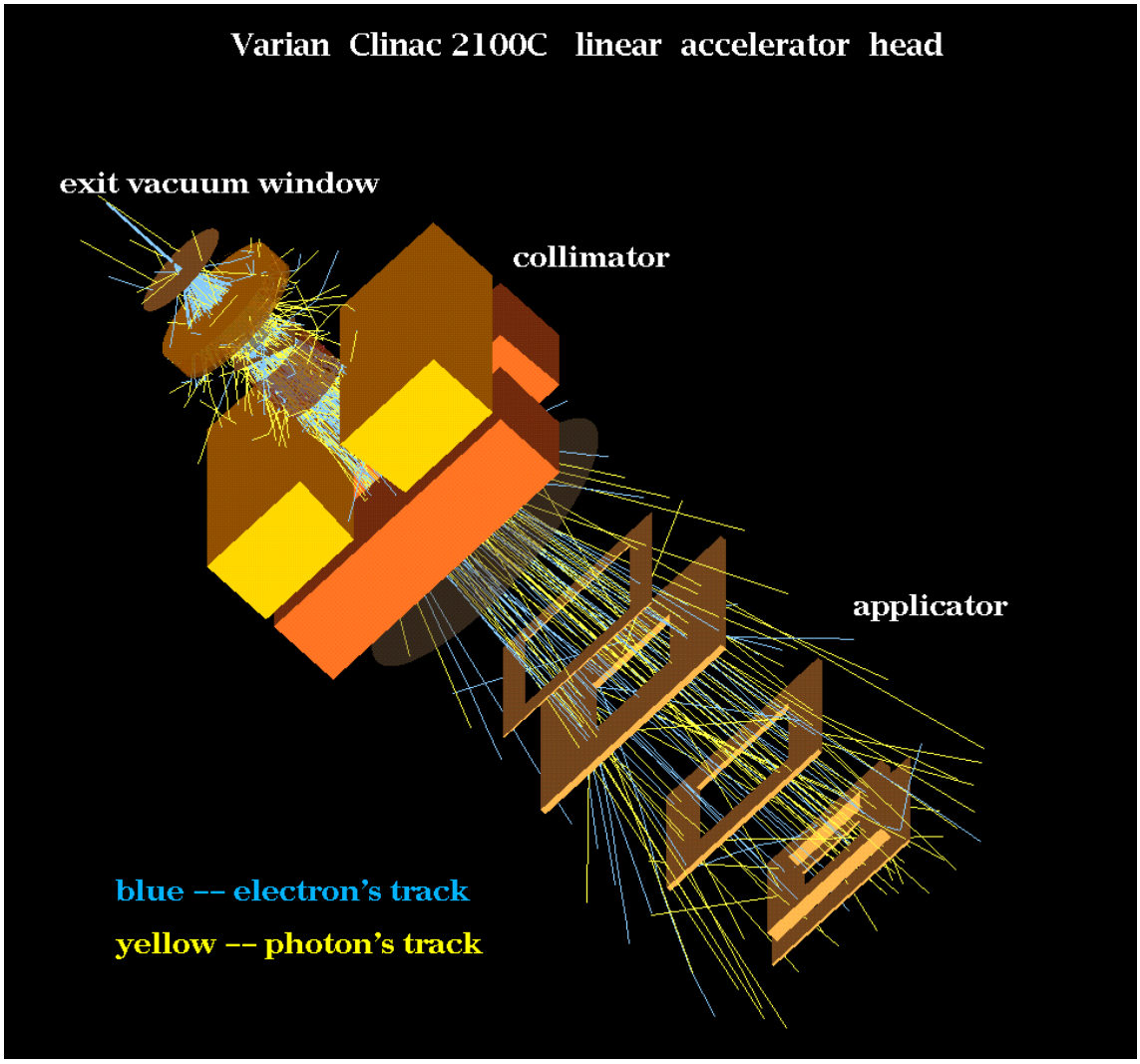

Figure 2: A 9 MeV electron beam from the Varian Clinac 2100C accelerator with type II applicator as shown by EGS_windows with about 100 histories. See section 3.3 for a detailed description.

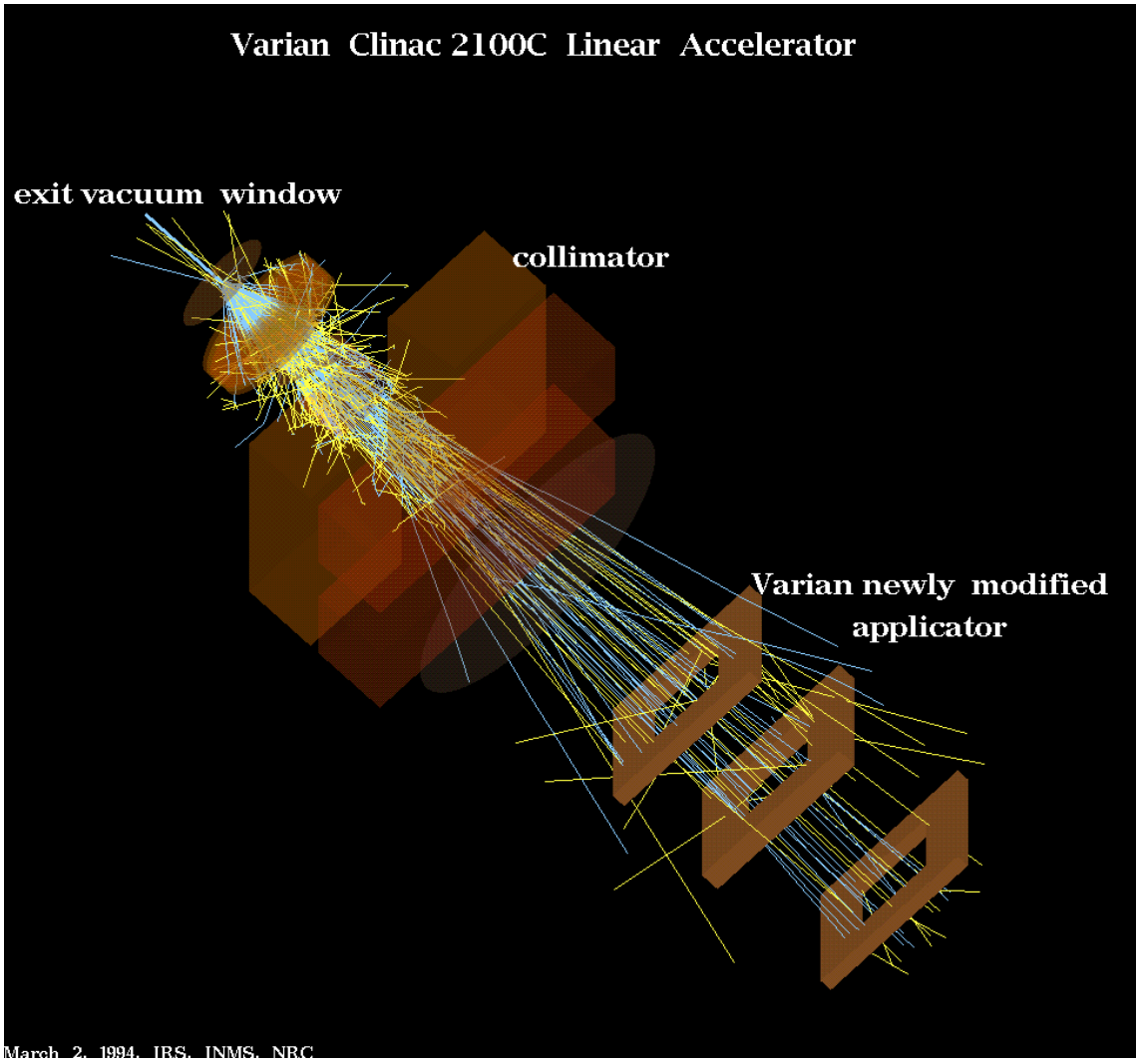

Figure 3: A 9 MeV electron beam from the Varian Clinac 2100C accelerator with type III applicator as shown by EGS_windows with about 100 histories. See section 3.3 for a detailed description.

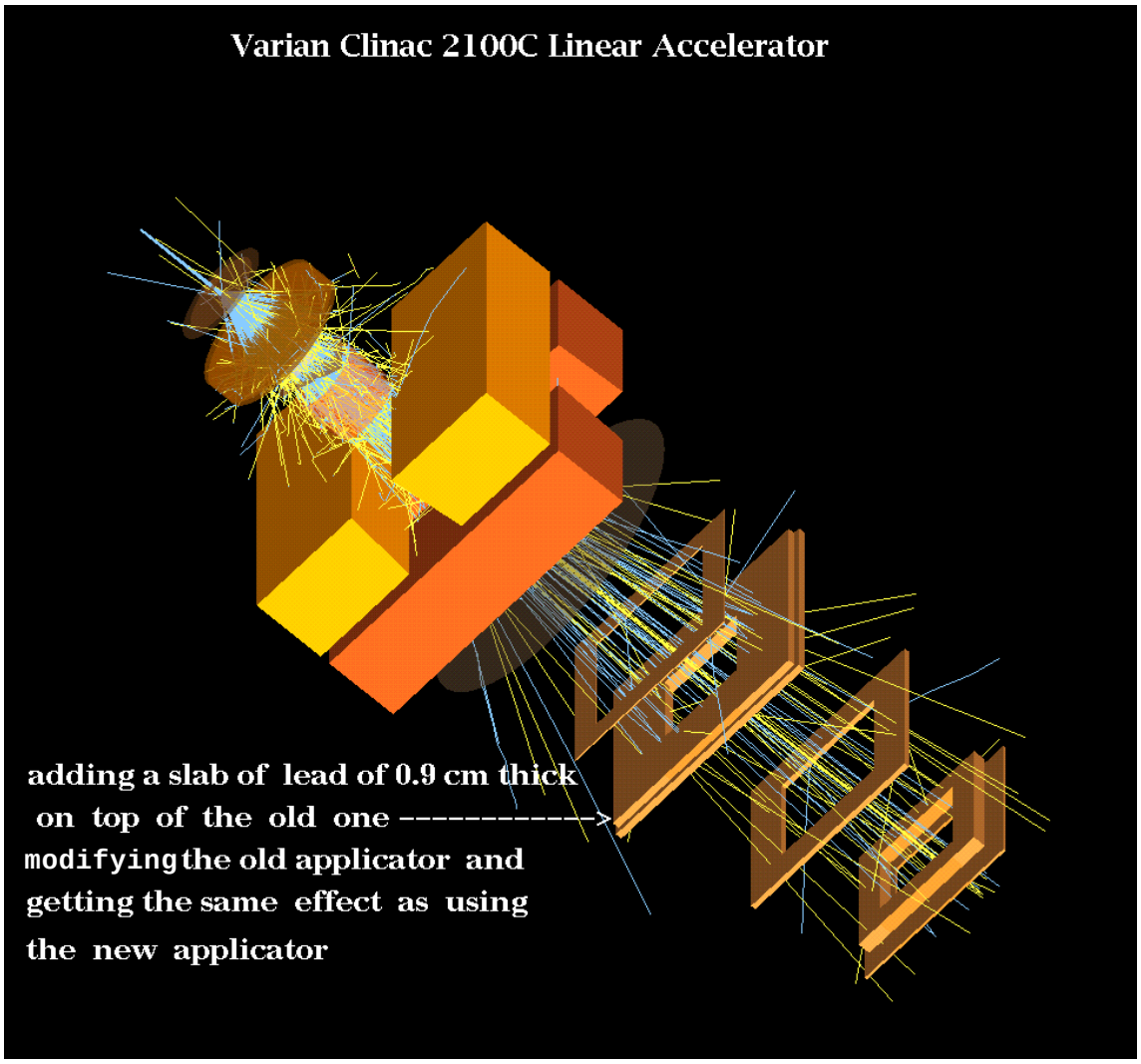

Figure 4: A 9 MeV electron beam from Varian Clinac 2100C accelerator with our modified applicator as shown by EGS_windows with about 100 histories. See section 3.3 for a detailed description.

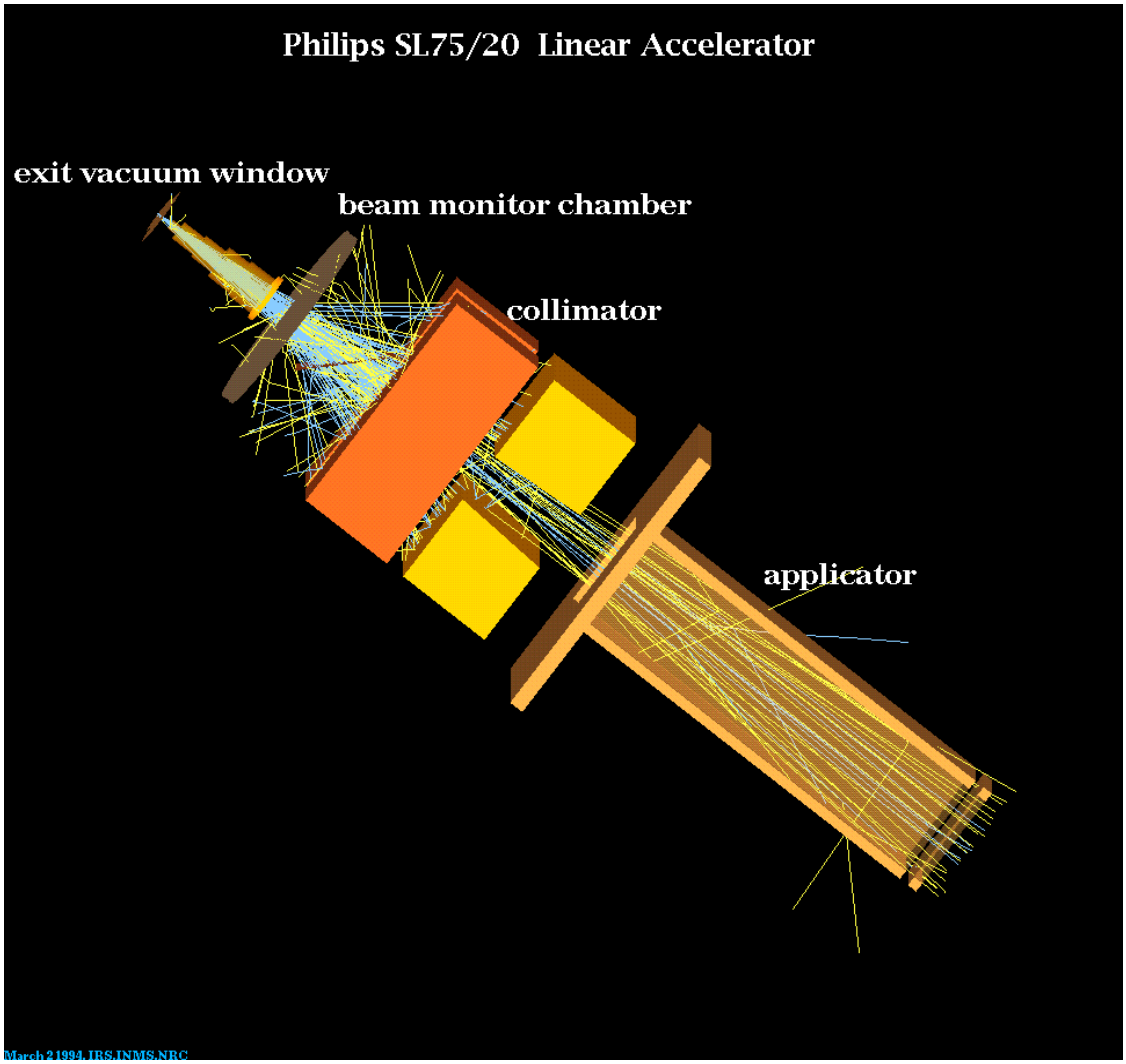

Figure 5: A 20 MeV electron beam from the Phillips SL75-20 accelerator as shown by EGS_windows with about 100 histories. See section 3.4 for a detailed description.

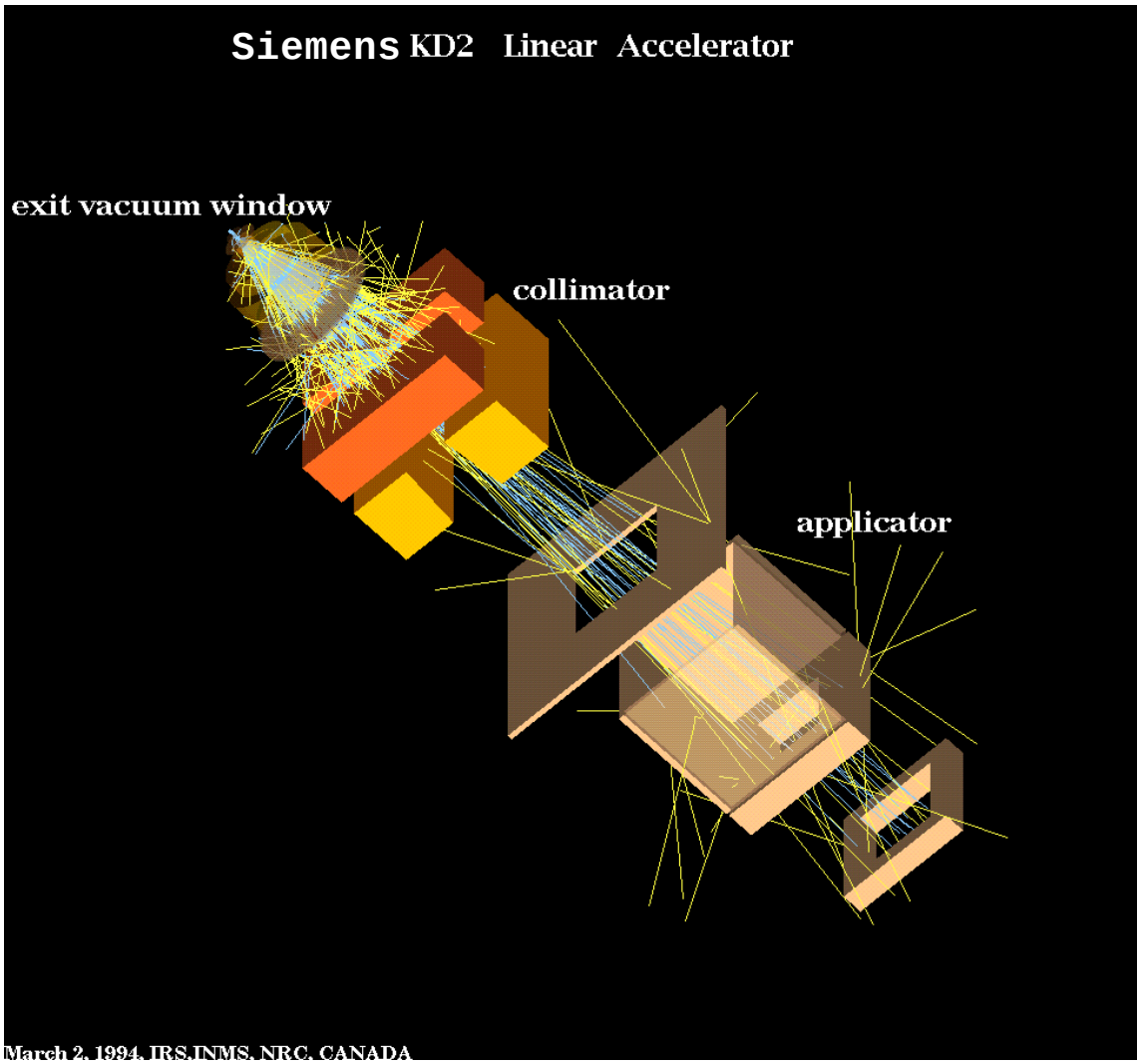

Figure 6: An 11 MeV electron beam from the Siemens KD2 accelerator as shown by EGS_windows with about 100 histories. See section 3.5 for a detailed description.

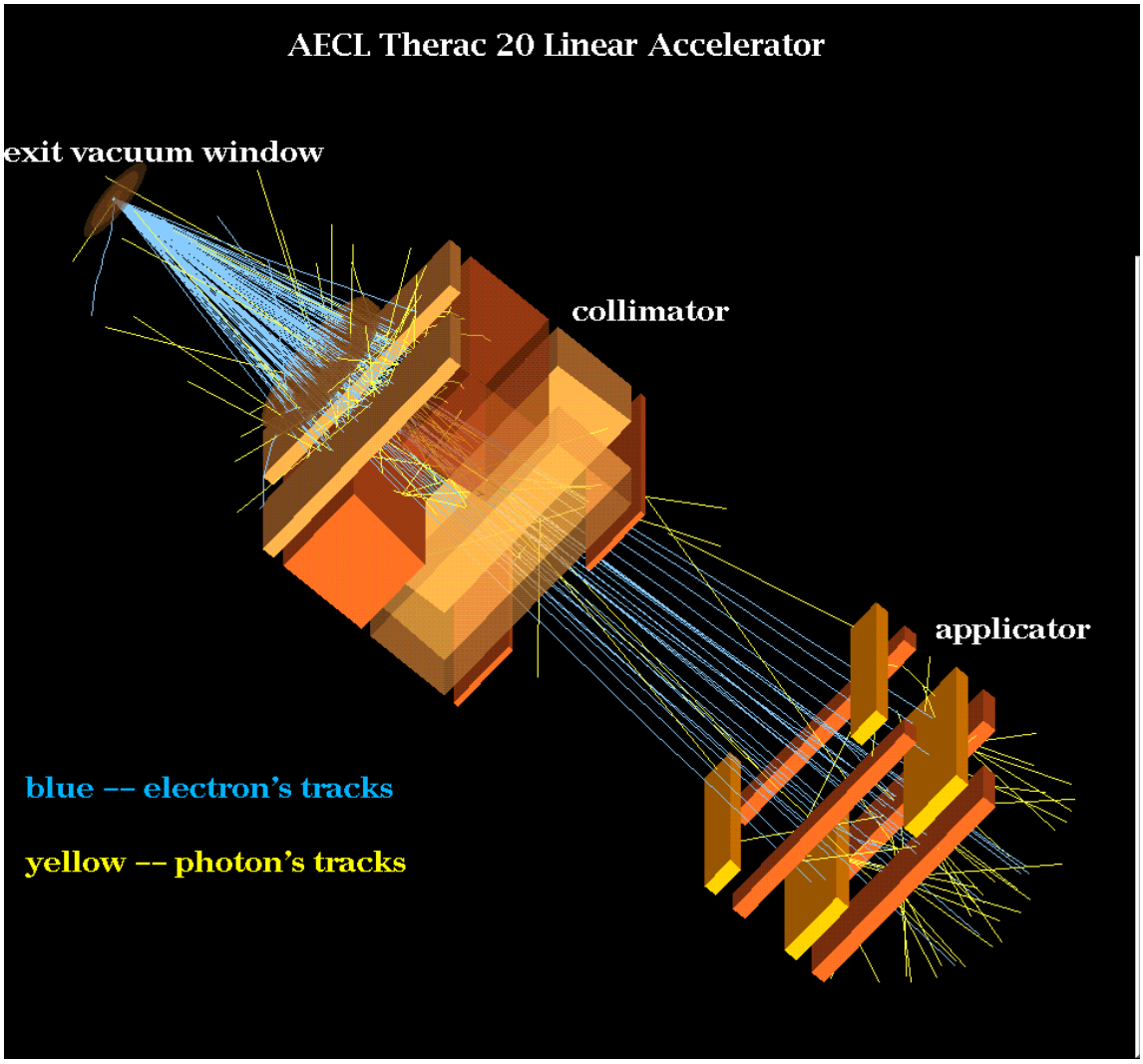

Figure 7: A 20 MeV electron beam from the AECL Therac 20 accelerator as shown by EGS_windows with about 100 histories. See section 3.6 for a detailed description.

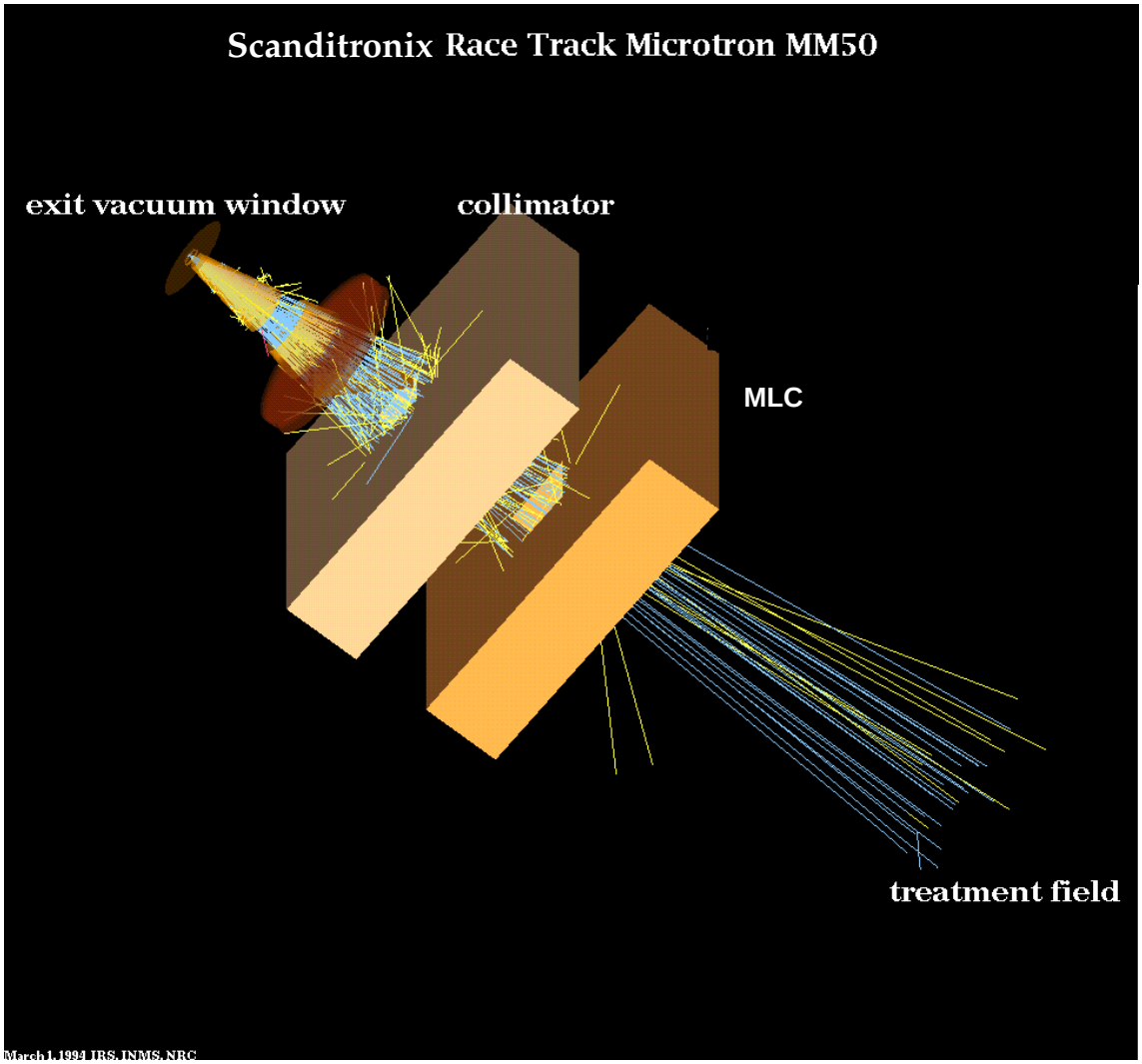

Figure 8: A 50 MeV electron beam from the Scanditronix MM50 accelerator as shown by EGS_windows with about 100 histories. See section 3.7 for a detailed description.

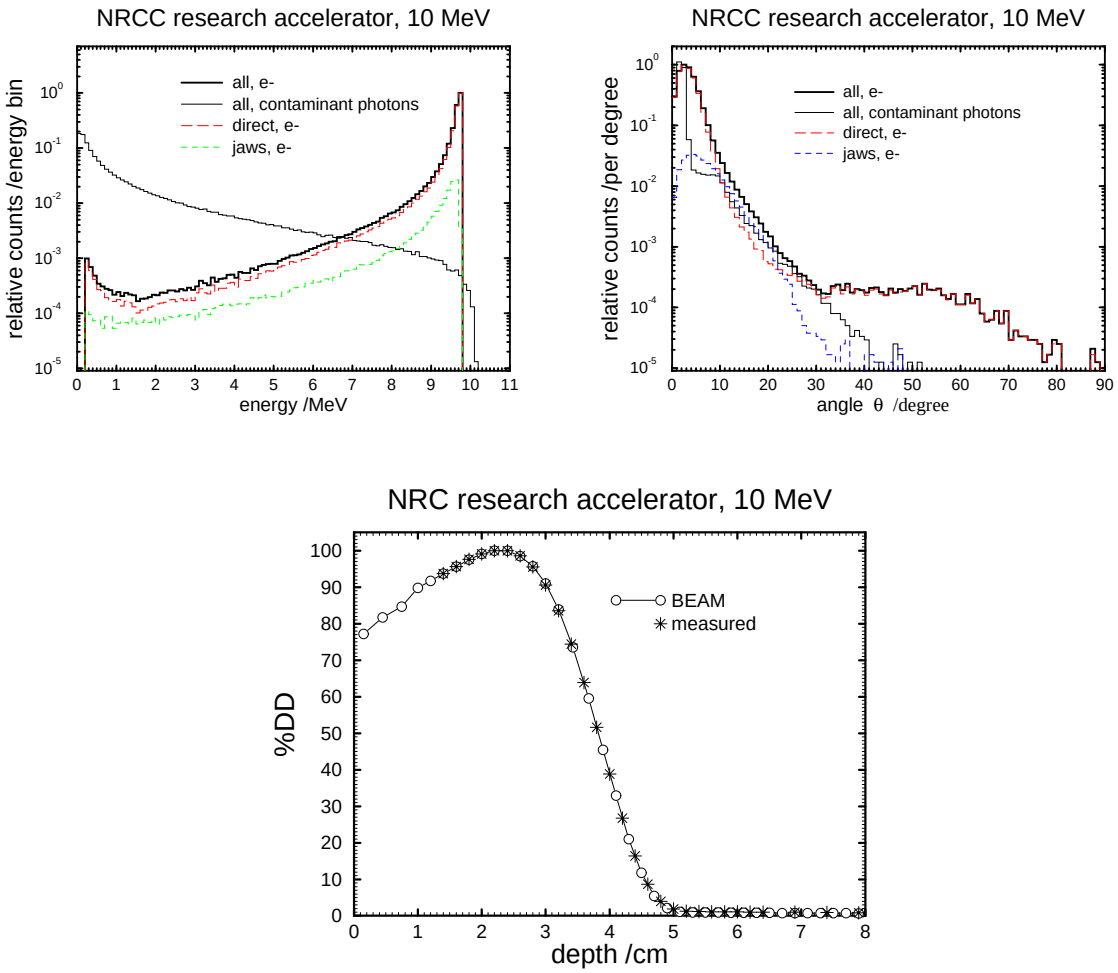

Figure 9: The energy spectra (upper left) and angular distributions (upper right) at the phantom surface and inside the 8×8 cm^2 field of a 10 MeV electron beam from NRCC accelerator. The ratio of the number of electrons to that of contaminant photons inside the field is $1 : 0.58$. The normalization values are 4.52×10^5 and 2.39×10^5 for spectra and angular distributions respectively. The lower figure is a comparison between calculated and measured central-axis depth-dose curves.

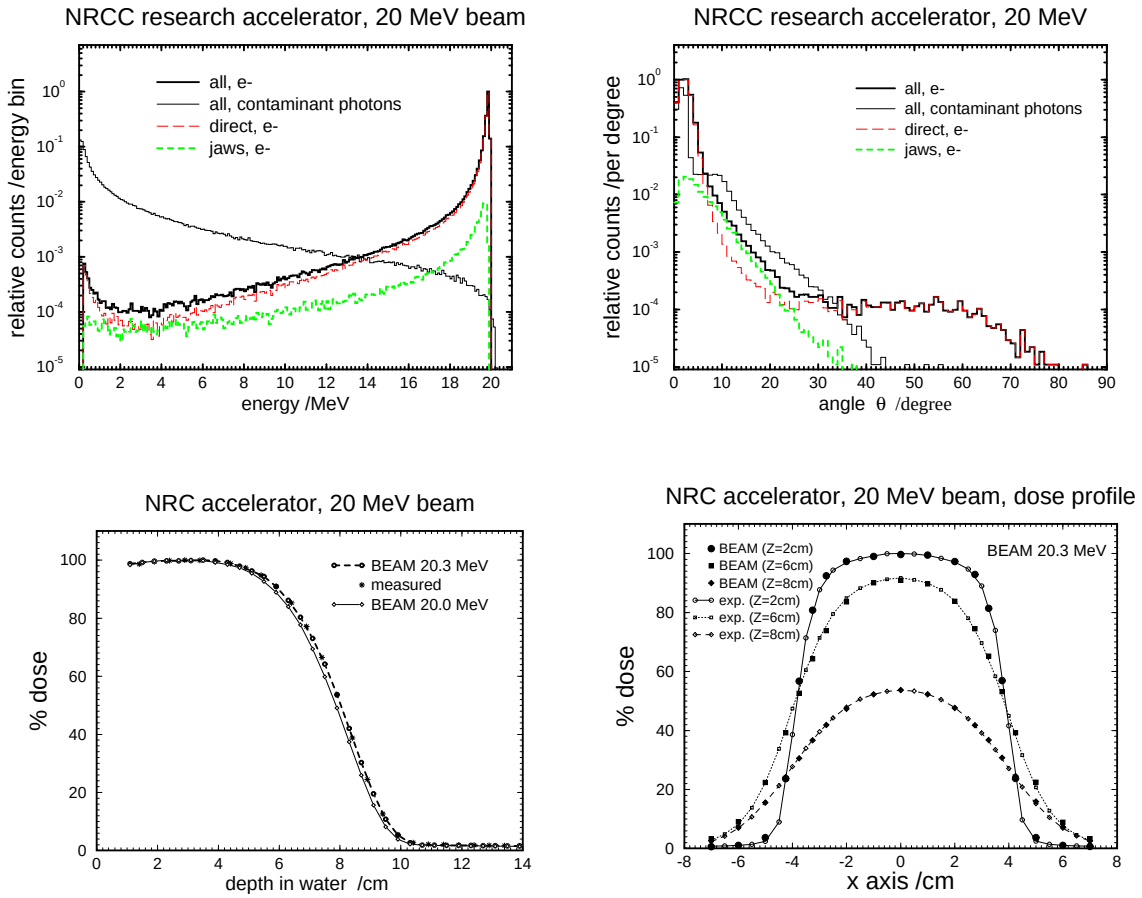

Figure 10: The energy spectra (upper left) and angular distributions (upper right) at the phantom surface and inside the 8×8 cm^2 field of a 20 MeV electron beam from the NRCC research accelerator. The energy used in the simulation is 20.3 MeV. Starting 10 M electron histories at the exit vacuum window there are 8.6×10^5 electrons and 4.3×10^5 photons inside field at the phantom surface. The ratio of the number of electrons to that of contaminant photons inside the field is 1 : 0.50. The normalization values are 4.11×10^5 and 2.78×10^5 for spectra and angular distributions respectively. The calculated and measured central-axis depth-dose curves (lower left), and dose profiles (lower right) at different depths in the 20 MeV electron beam.

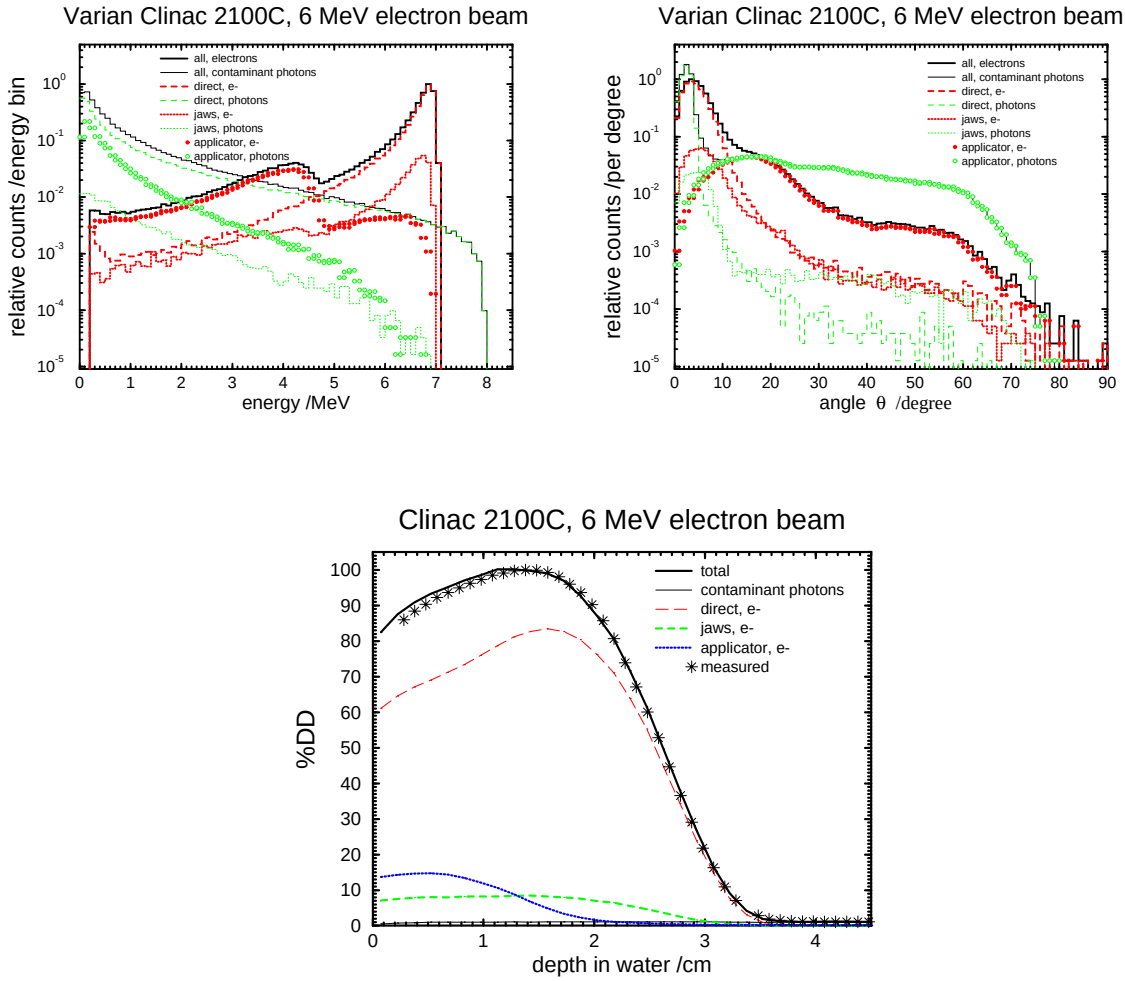

Figure 11: The energy spectra (upper left) and angular distributions (upper right) from various components at the phantom surface and inside the 10×10 cm^2 field of a 6 MeV electron beam from the Varian Clinac 2100C at the University of Wisconsin. The normalization values are 1.01×10^5 and 7.96×10^4 for the spectra and the angular distributions respectively. The lower figure is a comparison between measured and calculated depth-dose curves along with dose contributions from various components.

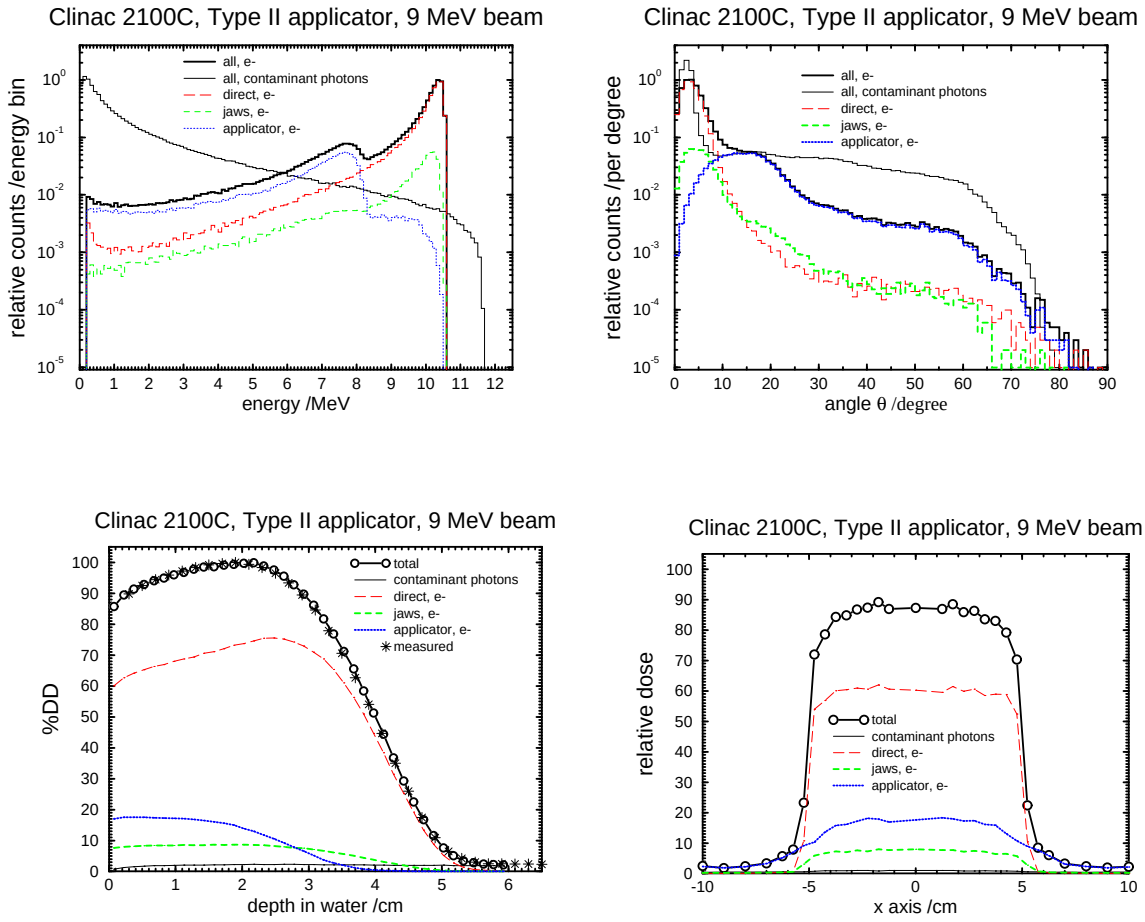

Figure 12: The energy spectra (upper left) and angular distributions (upper right) from various components at the phantom surface and inside the 10×10 cm^2 field of a 9 MeV electron beam from the Varian Clinac 2100C at the University of Wisconsin. The normalization values are 7.49×10^4 and 1.02×10^5 for the spectra and the angular distributions respectively. The lower figures are a comparison between measured and calculated depth-dose curves and the dose profiles at the surface (0.1 cm depth) from various components.

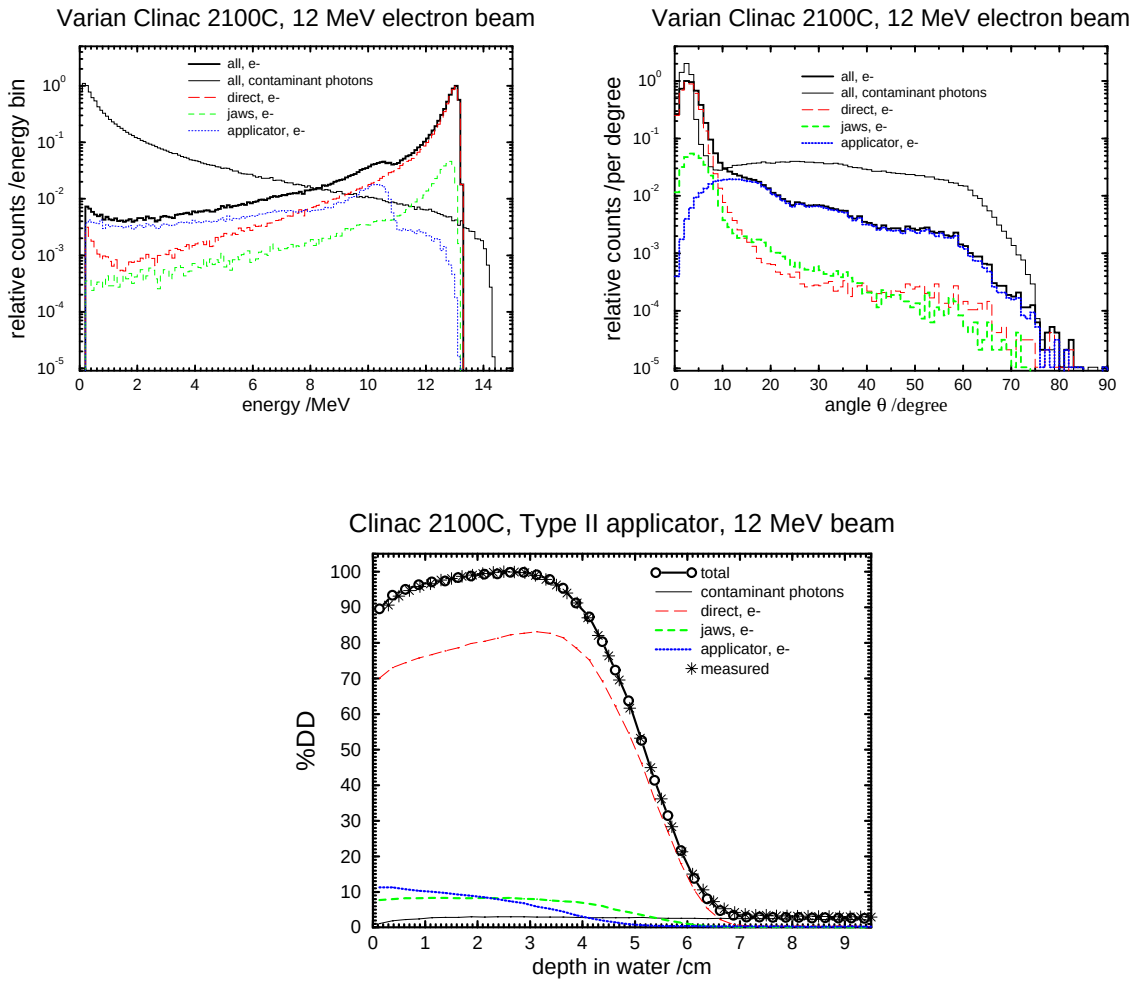

Figure 13: The energy spectra (upper left) and angular distributions (upper right) from various components at the phantom surface and inside the 10×10 cm^2 field of a 12 MeV electron beam from the Varian Clinac 2100C at the University of Wisconsin (Wisconsin Comprehensive Cancer Center in Madison). The normalization values are 6.28×10^4 and 9.58×10^4 for the spectra and the angular distributions respectively. The lower figure is a comparison between measured and calculated depth-dose curves along with dose contributions from various components.

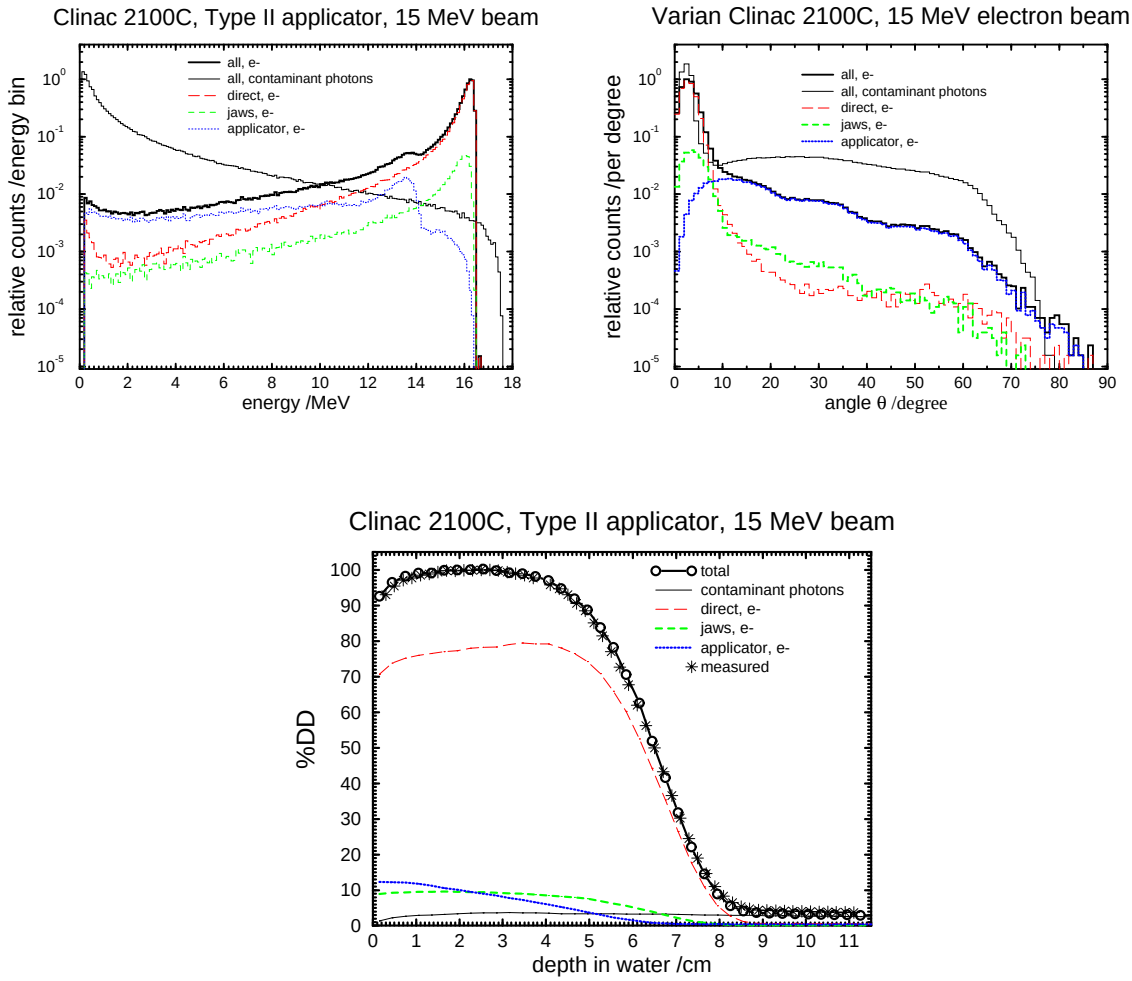

Figure 14: The energy spectra (upper left) and angular distributions (upper right) from various components at the phantom surface and inside the 10×10 cm^2 field of a 15 MeV electron beam from the Varian Clinac 2100C at the University of Wisconsin. The normalization values are 6.50×10^4 and 1.28×10^4 for the spectra and the angular distributions respectively. The lower figure is a comparison between measured and calculated depth-dose curves along with dose contributions from various components.

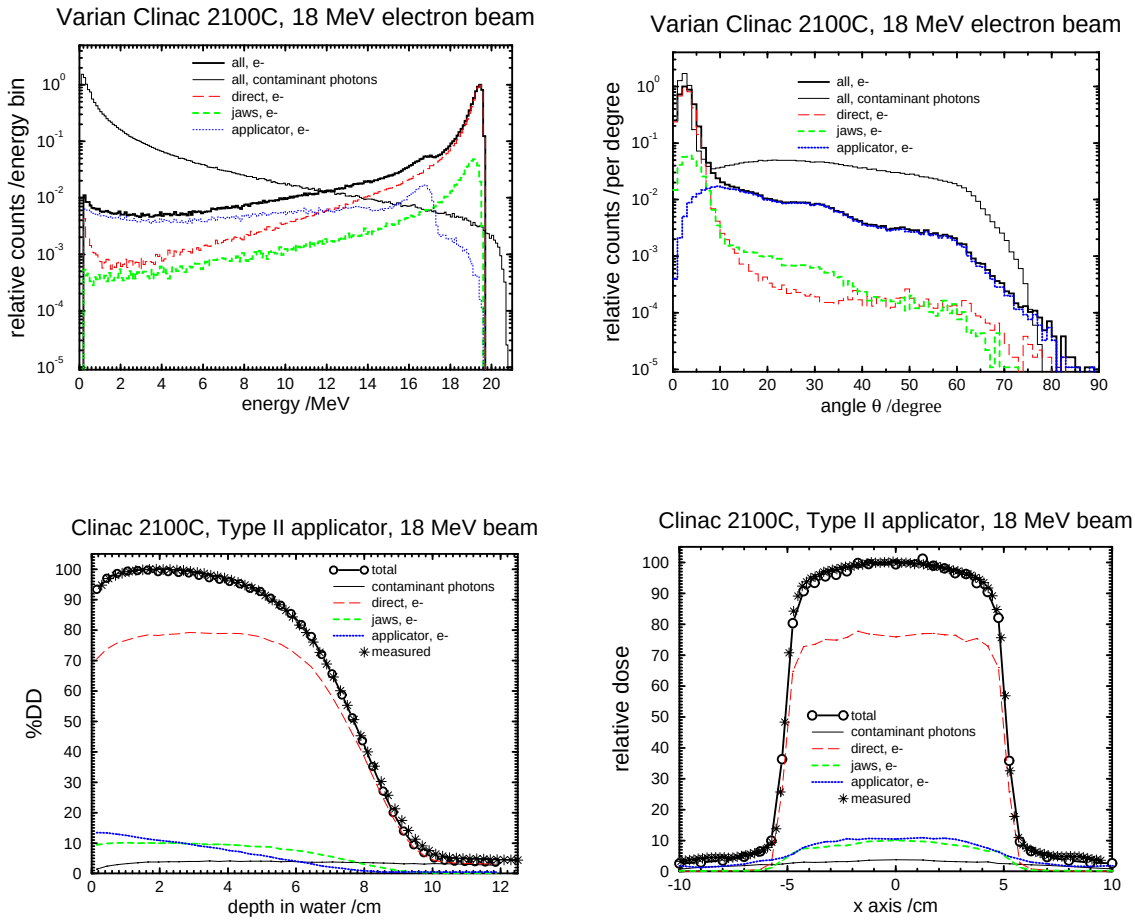

Figure 15: The energy spectra (upper left) and angular distributions (upper right) from various components at the phantom surface and inside the 10×10 cm^2 field of a 18 MeV electron beam from the Varian Clinac 2100C at the University of Wisconsin. The normalization values are 8.06×10^4 and 1.83×10^5 for the spectra and the angular distributions respectively. The lower figures are a comparison between measured and calculated depth-dose curves and dose profiles at d_{max} (1.9 cm depth) from various components.

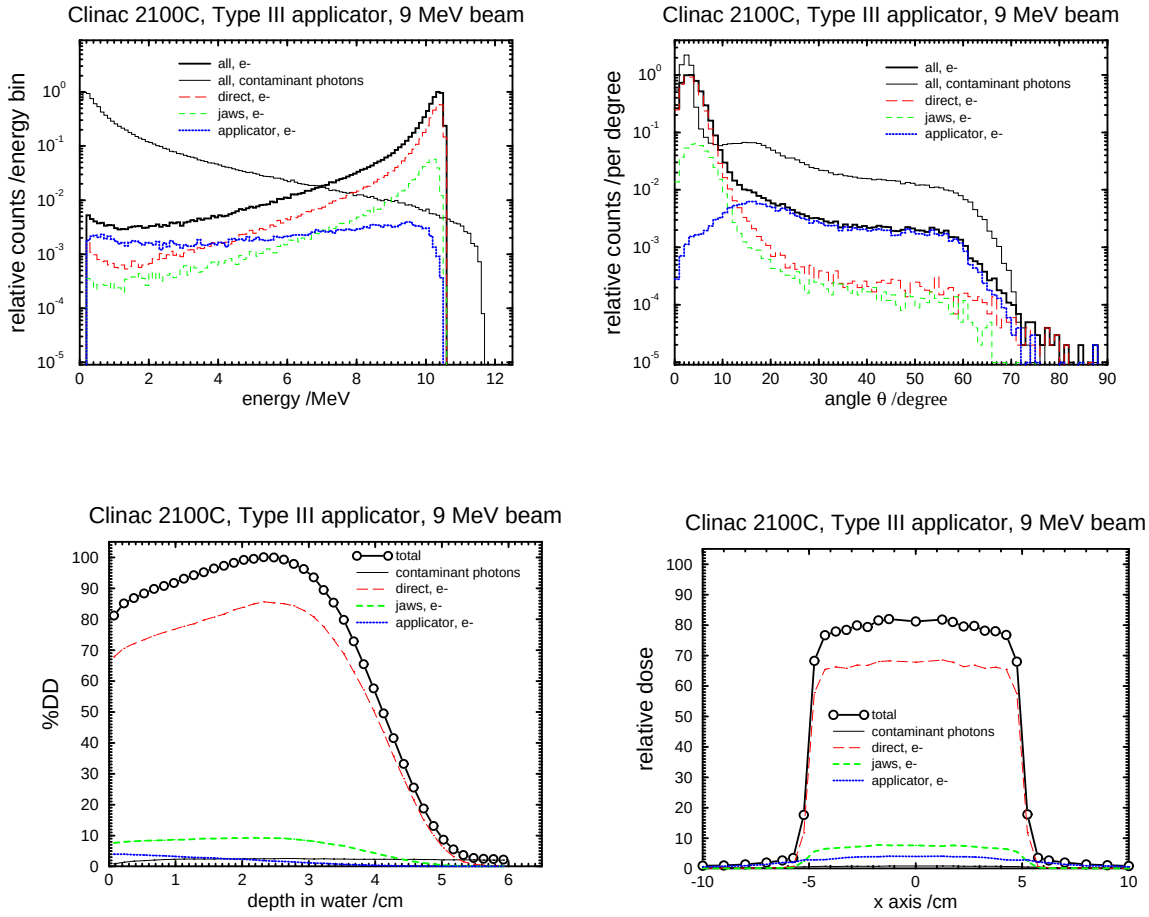

Figure 16: The energy spectra (upper left) and angular distributions (upper right) from various components at the phantom surface and inside the 10×10 cm^2 field of a 9 MeV electron beam from the Clinac 2100C with a newer applicator (Type III applicator). The normalization values are 7.56×10^4 and 1.01×10^5 for the spectra and the angular distributions respectively. The lower figures are the calculated central-axis depth-dose curves (left) and the dose profiles (right) at the surface (0.1 cm depth) from various components.

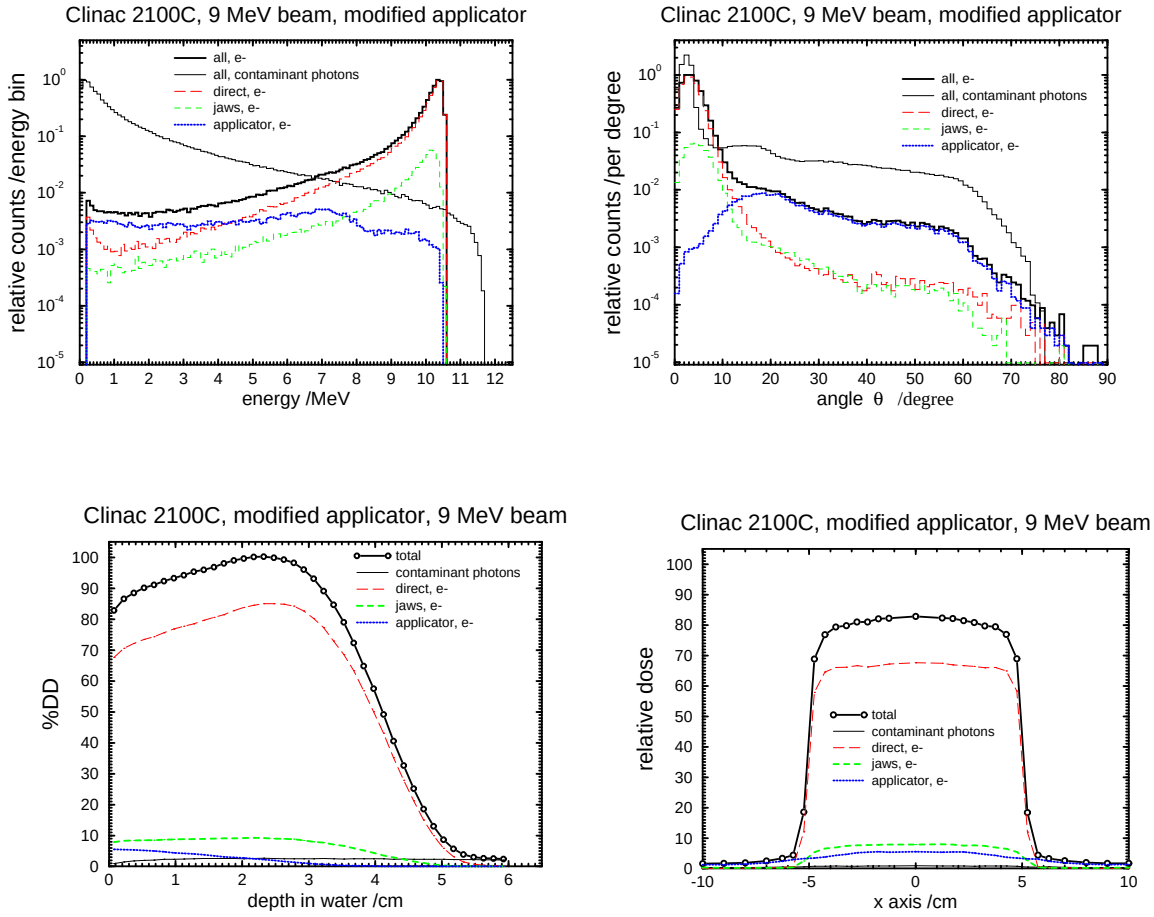

Figure 17: The energy spectra (upper left) and angular distributions (upper right) from various components at the phantom surface and inside the 10×10 cm^2 field of a 9 MeV electron beam from the Clinac 2100C with our modified applicator. The normalization values are 5.45×10^4 and 1.02×10^5 for the spectra and the angular distributions respectively. The lower figures are the calculated central-axis depth-dose curves (left) and dose profiles (right) at the surface (0.1 cm depth) from various components.

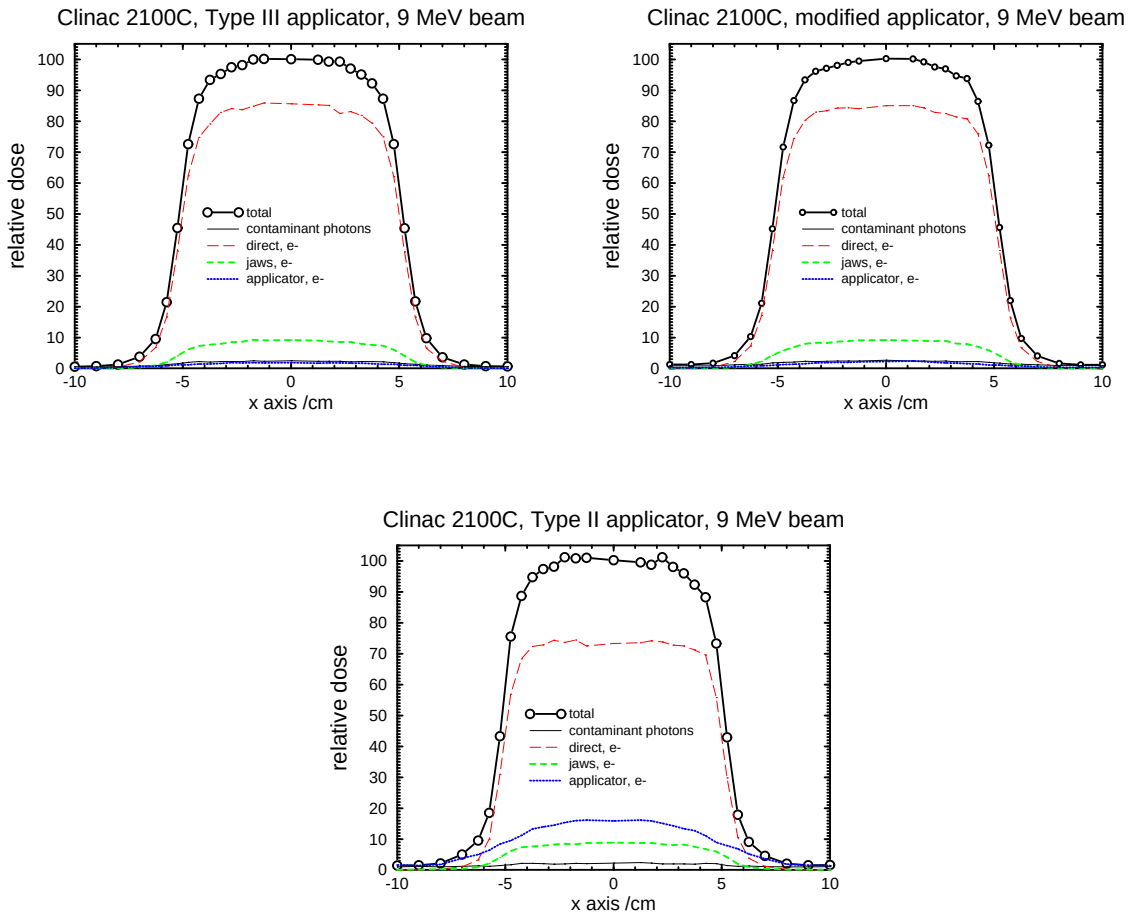

Figure 18: The calculated dose profile at d_{max} (2.3 cm depth) in a 9 MeV electron beam from the Varian Clinac 2100C with a Type III applicator (upper left). The dose profiles at d_{max} (2.3 cm depth) from various components in a 9 MeV electron beam from the Clinac 2100C with our modified applicator (upper right). The dose profiles at d_{max} (1.9 cm depth) from various components in a 9 MeV electron beam from the Varian Clinac 2100C with a Type II applicator (lower). It can be seen that our simply modified applicator has virtually identical dose profiles at d_{max} to that of the new design applicator (Type III), even for dose components.

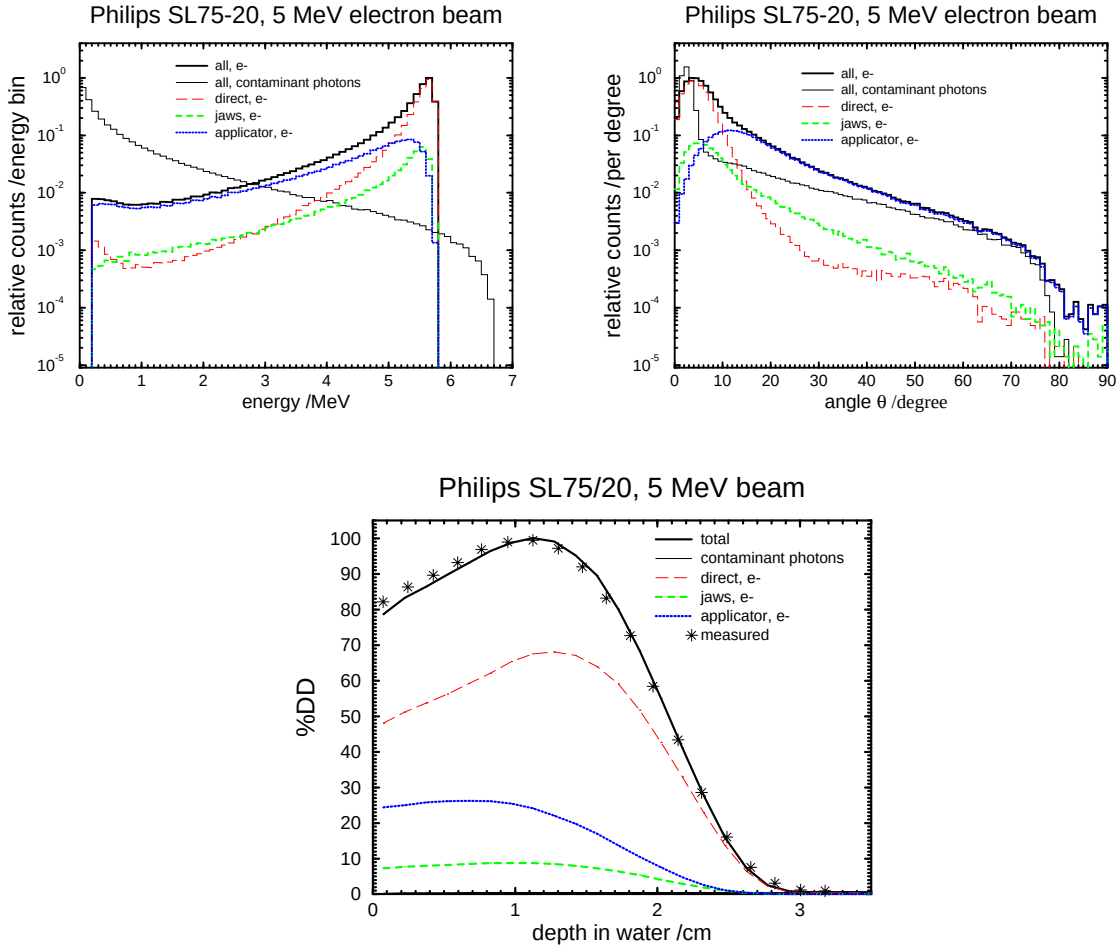

Figure 19: The energy spectra (upper left) and angular distributions (upper right) from various components at the phantom surface and inside the 10×10 cm^2 field of a 5 MeV electron beam from the Philips SL75-20 at Leeds University[13]. The normalization values are 2.47×10^5 and 1.42×10^5 for the spectra and the angular distributions respectively. The lower figure is a comparison between measured and calculated depth-dose curves along with dose contributions from various beam defining components.

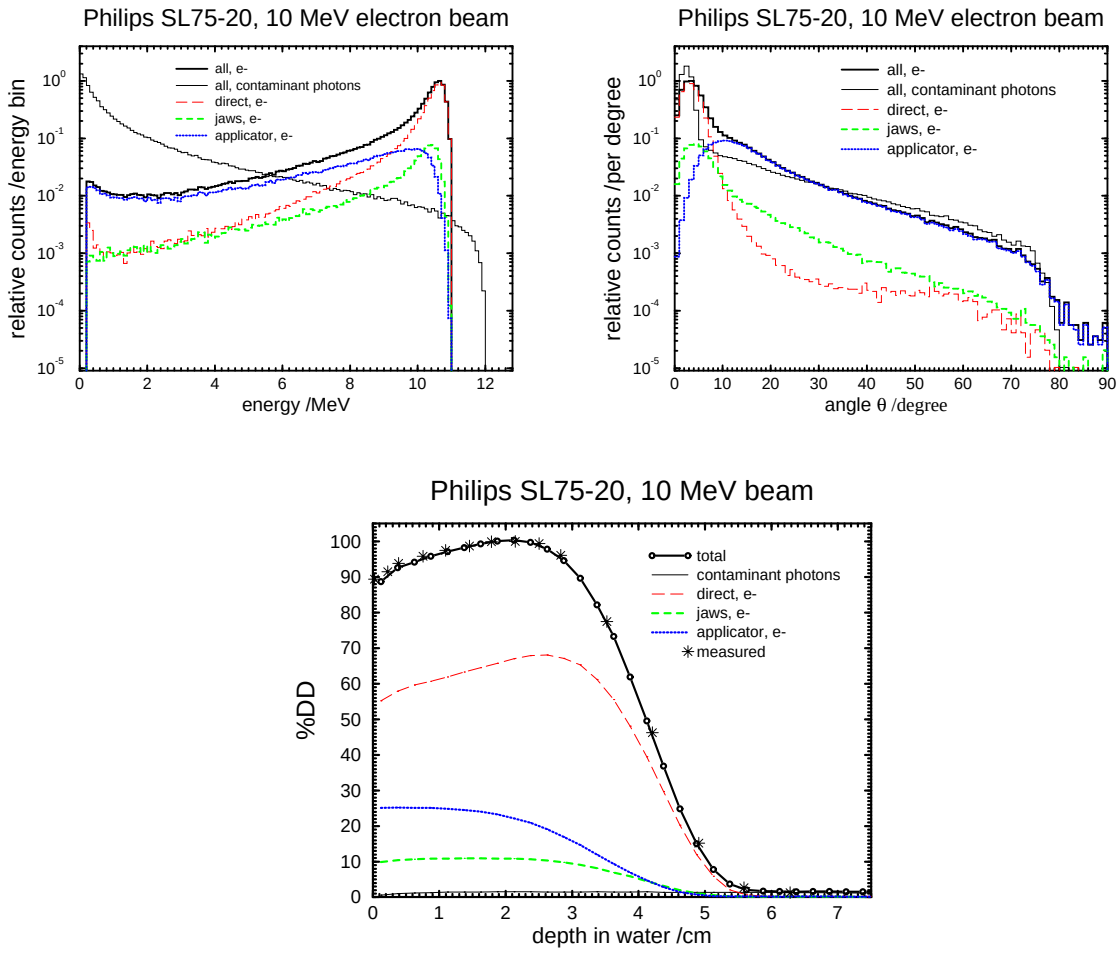

Figure 20: The energy spectra (upper left) and angular distributions (upper right) from various components at the phantom surface and inside the 10×10 cm^2 field of a 10 MeV electron beam from the Philips SL75-20 at Leeds University[13]. The normalization values are 1.22×10^5 and 1.94×10^5 for the spectra and the angular distributions respectively. The lower figure is a comparison between measured and calculated depth-dose curves along with dose contributions from various beam defining components.

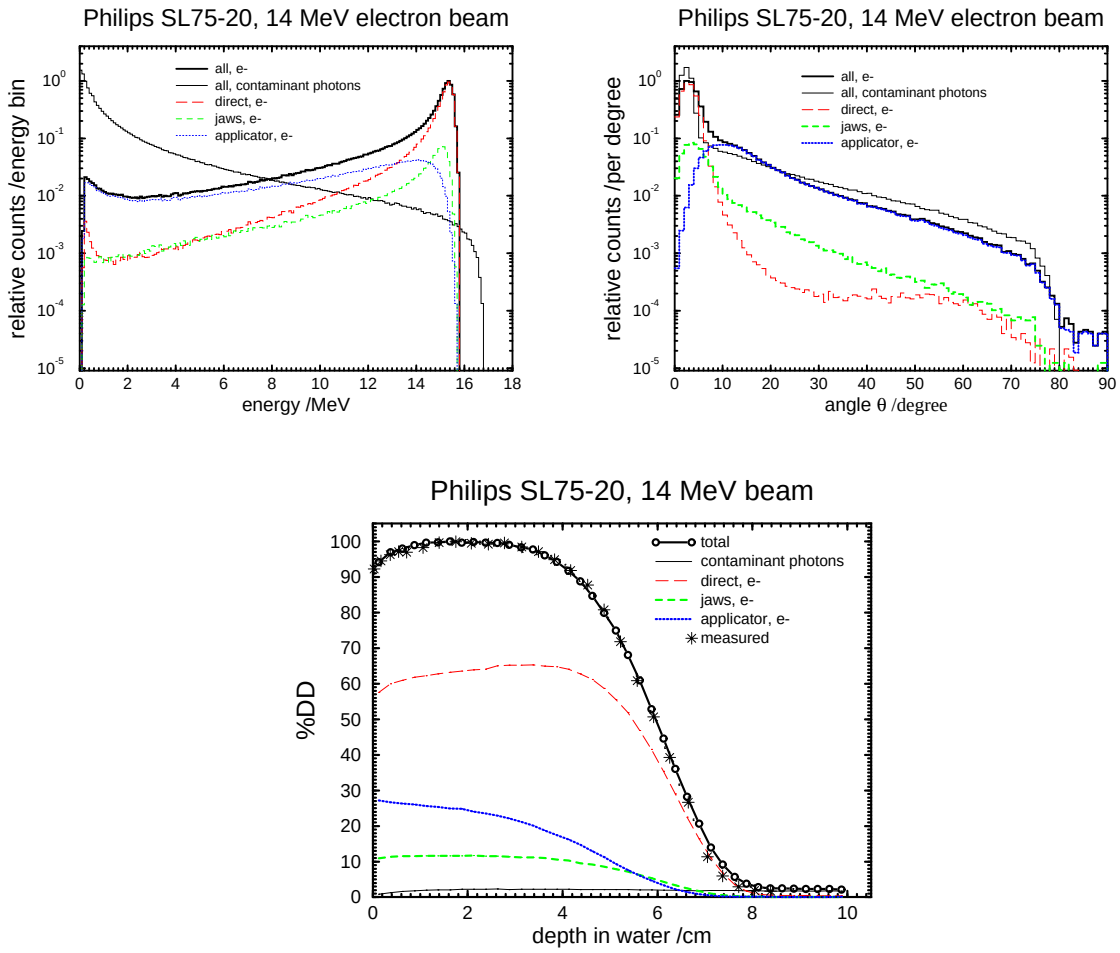

Figure 21: The energy spectra (upper left) and angular distributions (upper right) from various components at the phantom surface and inside the 10×10 cm^2 field of a 14 MeV electron beam from the Philips SL75-20 at Leeds University[13]. The normalization values are 1.58×10^5 and 3.24×10^5 for the spectra and the angular distributions respectively. The lower figure is a comparison between measured[13] and calculated depth-dose curves along with dose contributions from various beam defining components.

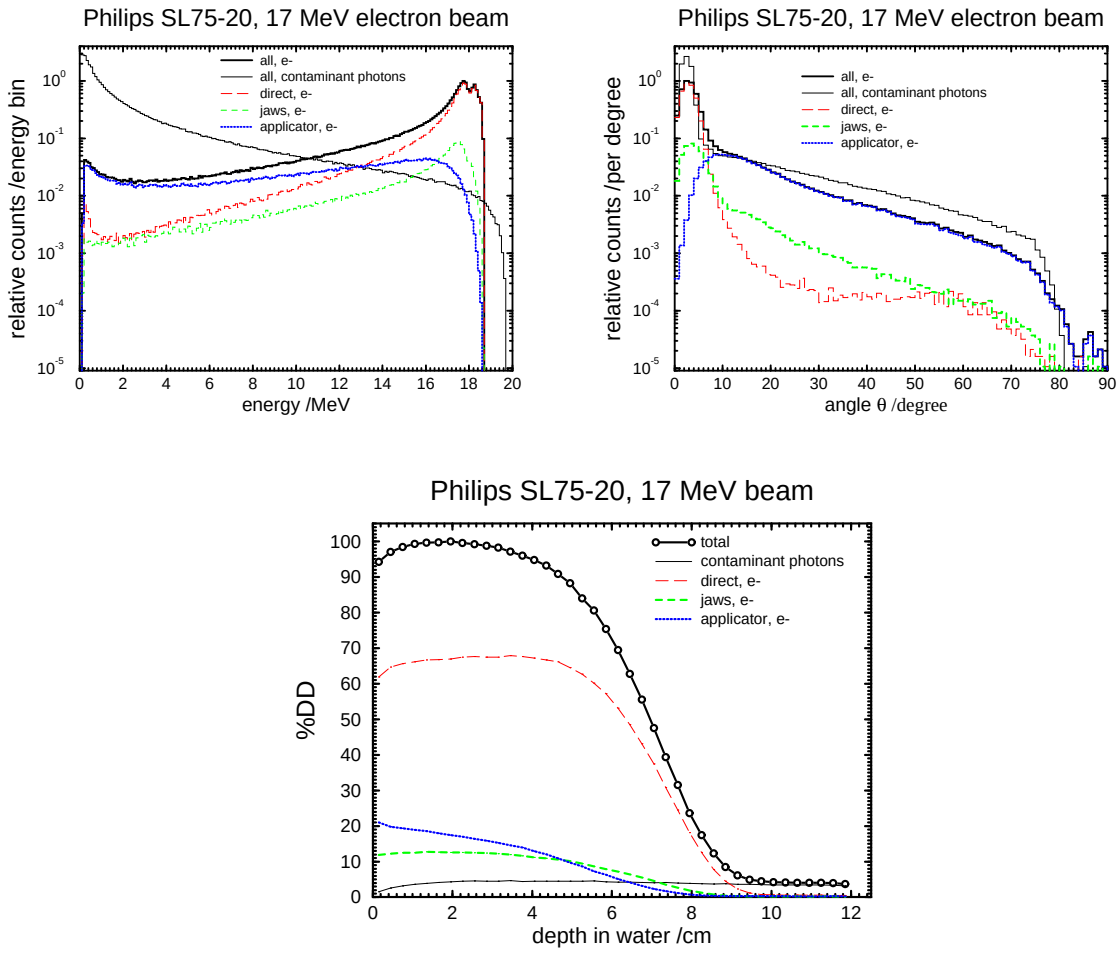

Figure 22: The energy spectra (upper left) and angular distributions (upper right) from various components at the phantom surface and inside the 10×10 cm^2 field of a 17 MeV electron beam from the Philips SL75-20 at Leeds University[13]. The normalization values are 3.83×10^4 and 1.88×10^5 for the spectra and the angular distributions respectively. The lower figure shows calculated depth-dose curves along with dose contributions from various beam defining components.

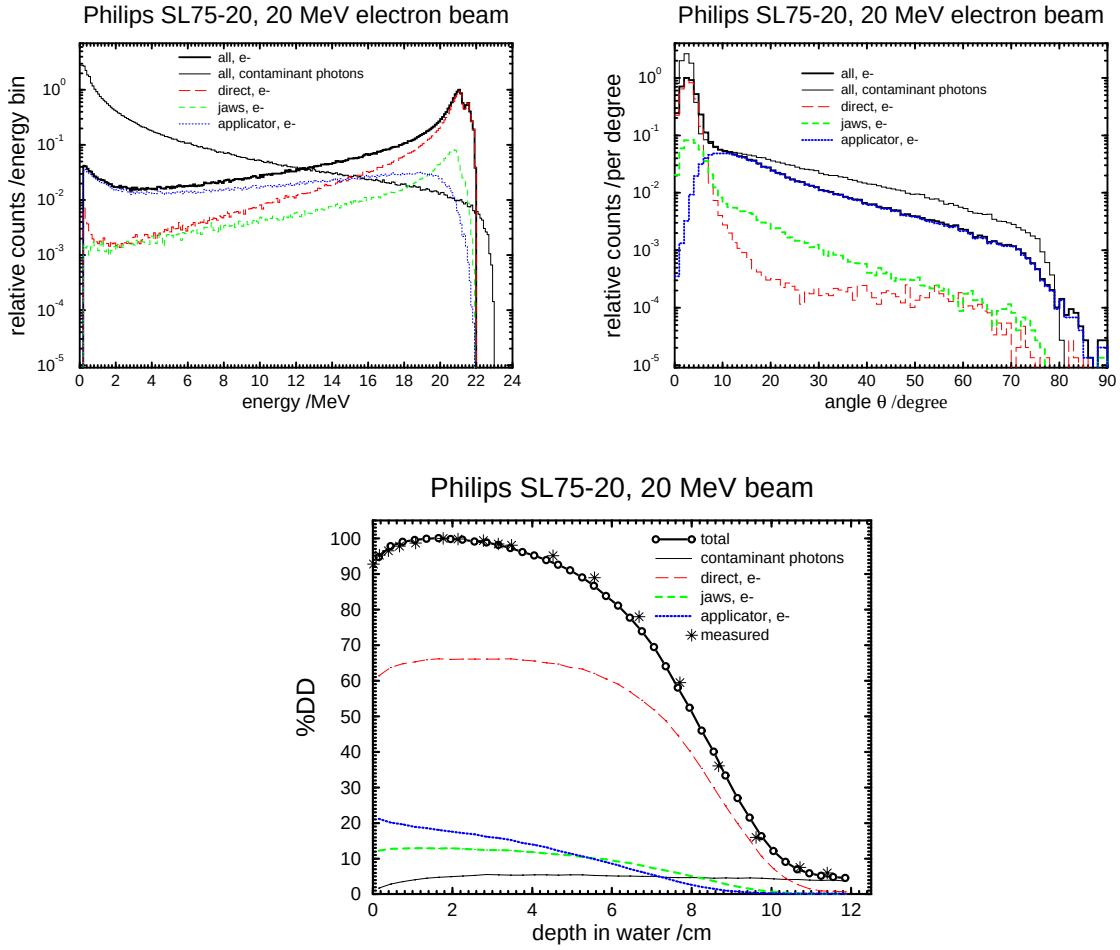

Figure 23: The energy spectra (upper left) and angular distributions (upper right) from various components at the phantom surface and inside the 10×10 cm^2 field of a 20 MeV electron beam from the Philips SL75-20 at Leeds University. The normalization values are 3.48×10^4 and 1.48×10^5 for the spectra and the angular distributions respectively. The lower figure is a comparison between measured and calculated depth-dose curves along with dose contributions from various beam defining components.

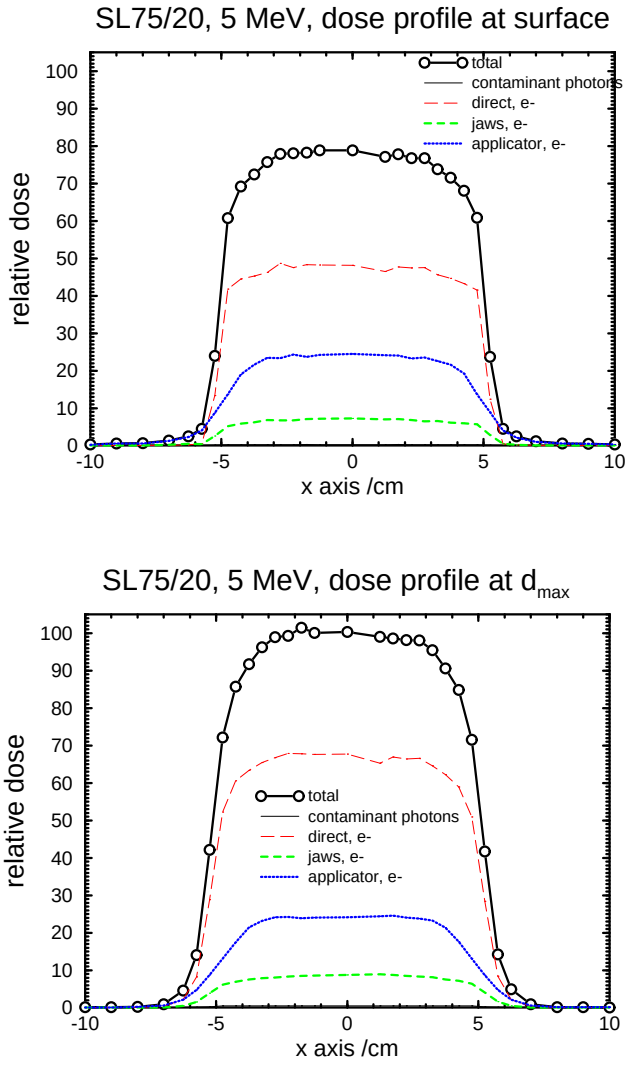

Figure 24: The calculated dose profiles at the surface (0.1 cm depth) (upper) and at d_{max} (1.1 cm depth) (lower) of a 5 MeV electron beam from the Philips SL75-20 at Leeds University for various dose components.

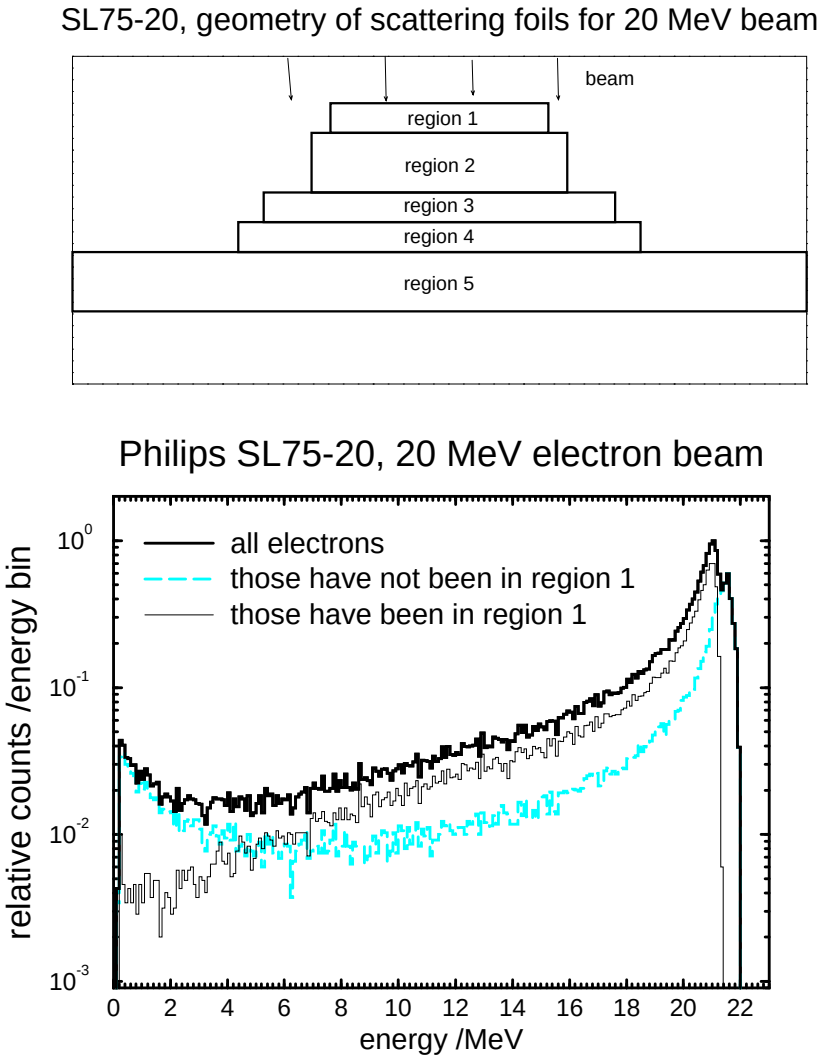

Figure 25: Geometry of scattering foils (upper) for the 20 MeV beam of the SL75-20, where regions 1 to 5 are thin metal cylinders. Region 1 has a radius of 0.725 cm and a thickness of 0.0127 cm. The distance between the scattering foils and the exit vacuum window is about 15 cm. Electron spectra at the phantom surface are shown in the lower panel. Those electrons which have been in region 1 lose more energy because they have to pass through the extra thickness of region 1.

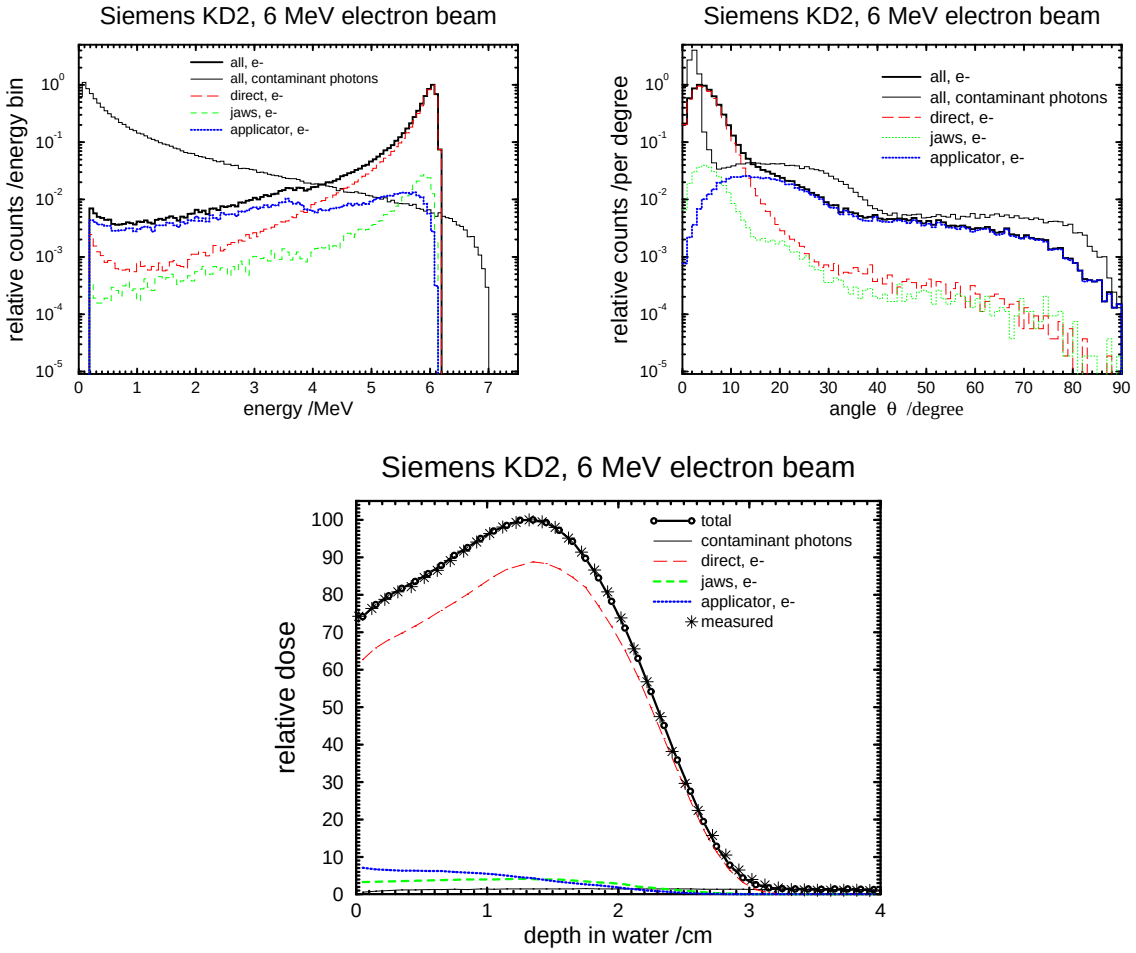

Figure 26: The energy spectra (upper left) and angular distributions (upper right) from various components at the phantom surface and inside the 10×10 cm^2 field of a 6 MeV electron beam from Siemens KD2 at the General Hospital in Ottawa. The normalization values are 5.78×10^4 and 5.37×10^4 for the spectra and the angular distributions respectively. The lower figure is a comparison between measured and calculated depth-dose curves (lower left) and dose profiles along with various dose components.

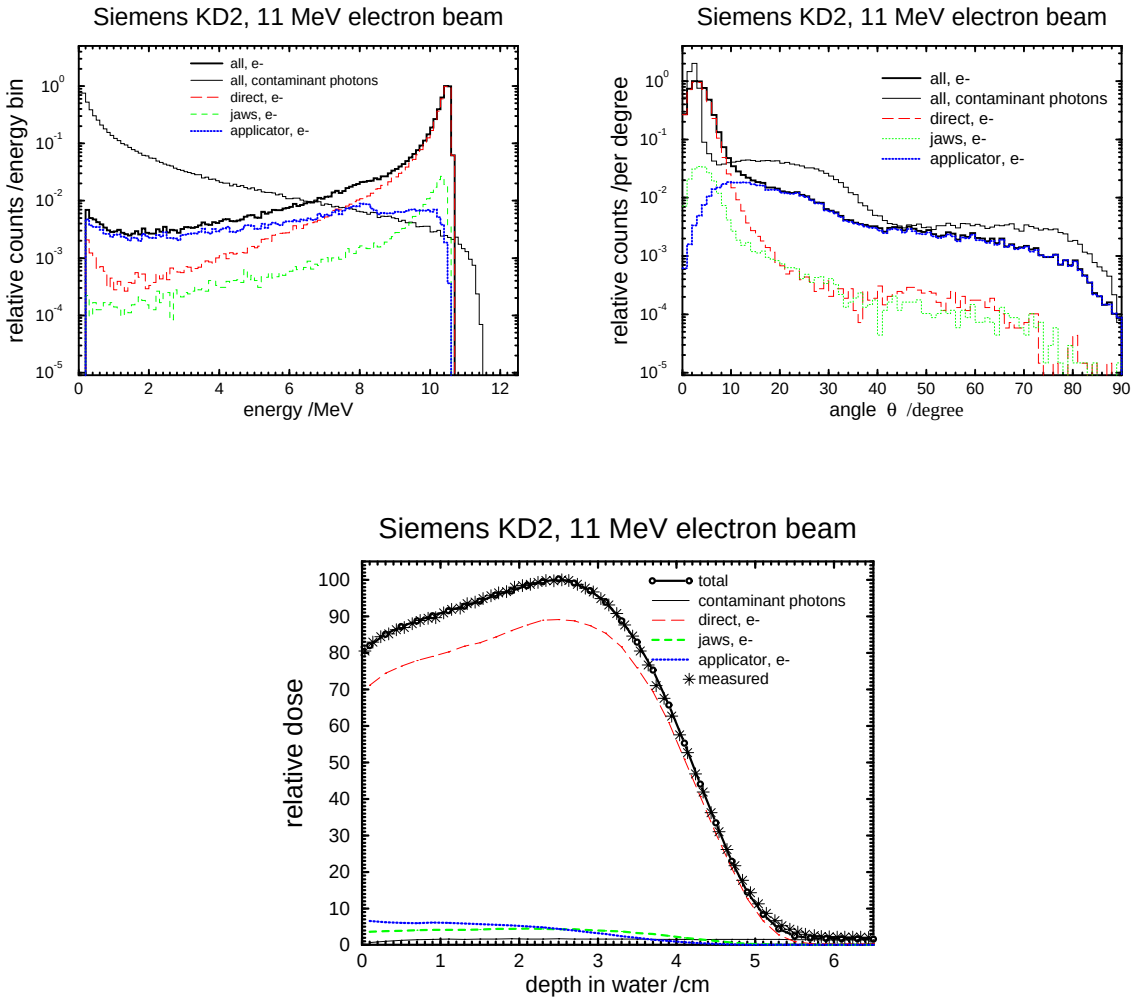

Figure 27: The energy spectra (upper left) and angular distributions (upper right) from various components at the phantom surface and inside the 10×10 cm^2 field of an 11 MeV electron beam from Siemens KD2 at the General Hospital in Ottawa. The normalization values are 7.60×10^4 and 6.88×10^4 for the spectra and the angular distributions respectively. The lower figure is a comparison between measured and calculated depth-dose curves along with various dose components.

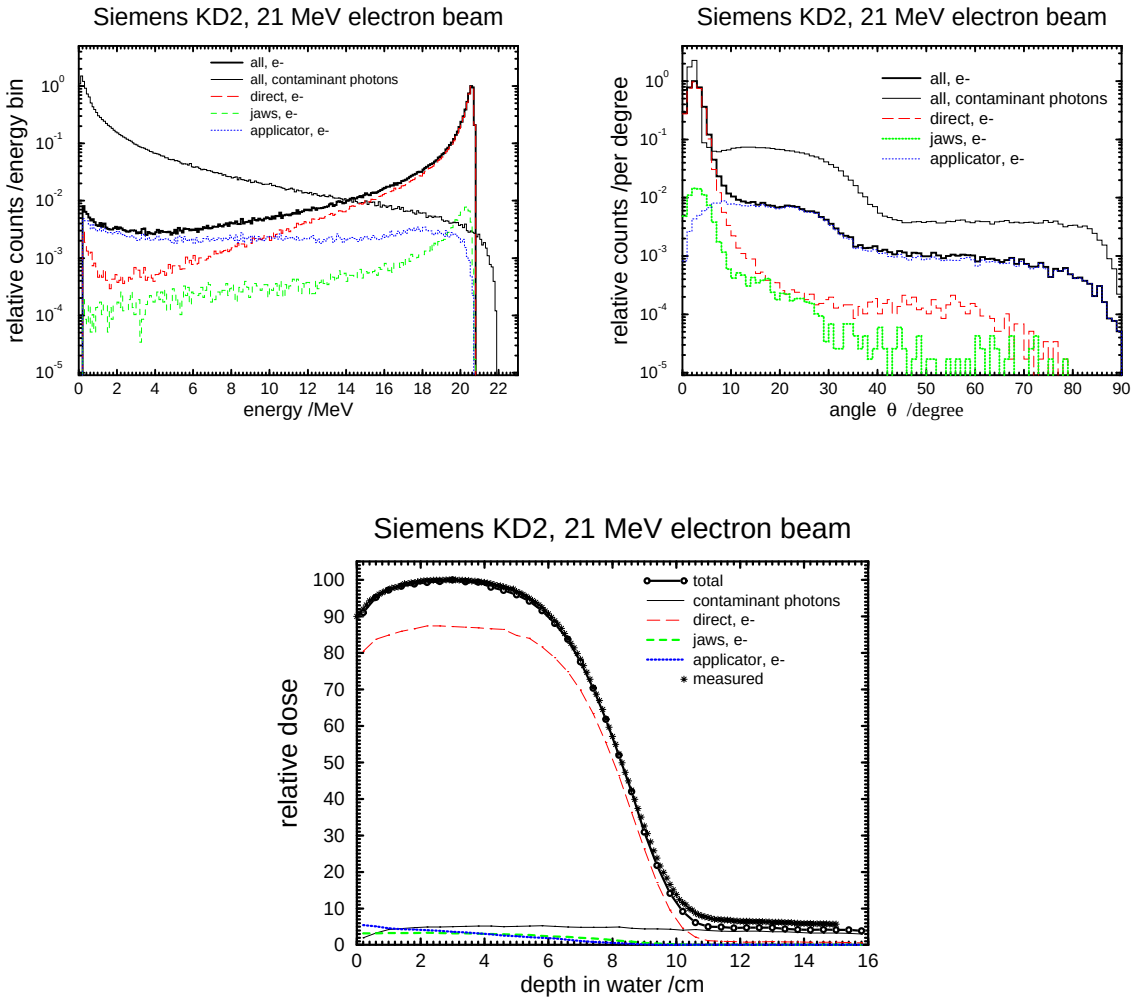

Figure 28: The energy spectra (upper left) and angular distributions (upper right) from various components at the phantom surface and inside the 10×10 cm^2 field of a 21 MeV electron beam from a Siemens KD2 in the Netherlands. The normalization values are 5.69×10^4 and 1.17×10^5 for the spectra and the angular distributions respectively. The lower figure is a comparison between measured and calculated central-axis depth-dose curves from various dose components.

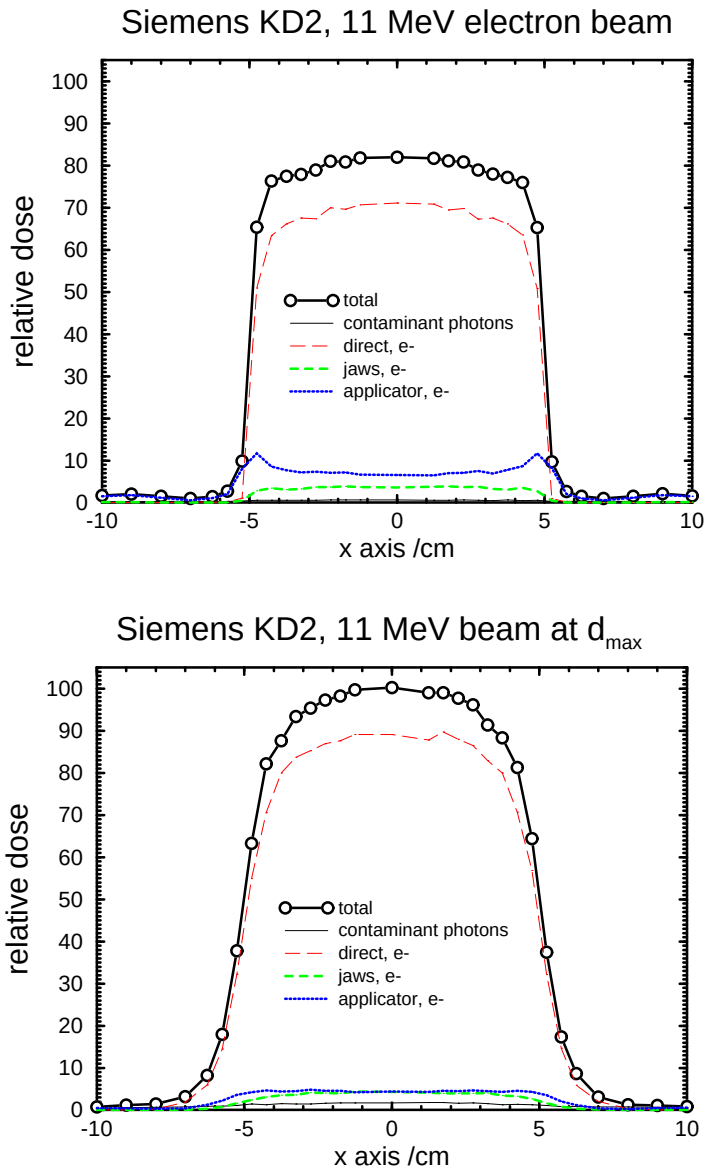

Figure 29: Calculated dose profiles at the phantom surface (upper) and at the depth of d_{max} (lower) from various dose components for the 11 MeV electron beam from the Siemens KD2 at the General Hospital in Ottawa.

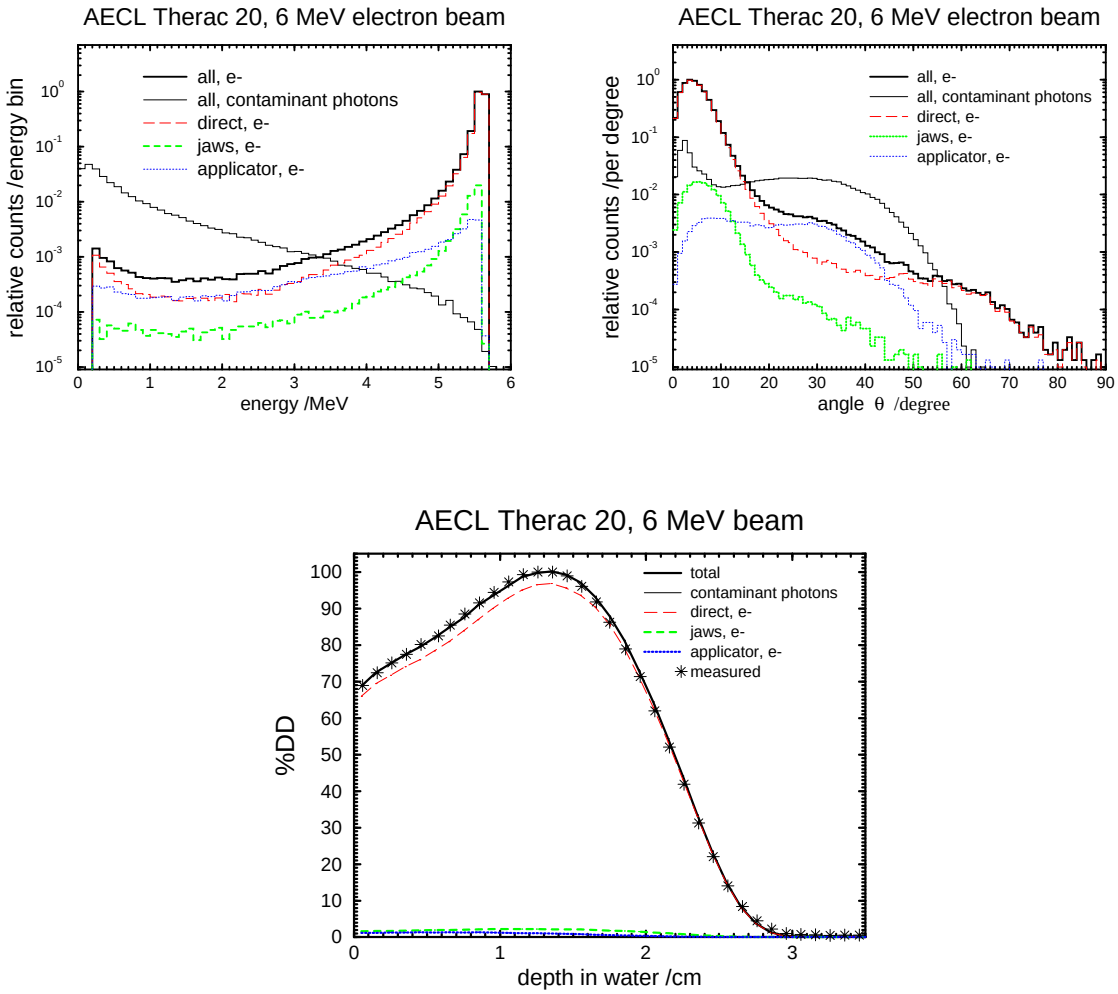

Figure 30: The energy spectra (upper left) and angular distributions (upper right) from various components at the phantom surface and inside the 10×10 cm^2 field of a 6 MeV electron beam from the AECL Therac 20. The normalization values are 9.63×10^5 and 3.02×10^5 for the spectra and the angular distributions respectively. The lower figure is a comparison between measured and calculated depth-dose curves along with dose components contributed from each beam defining component.

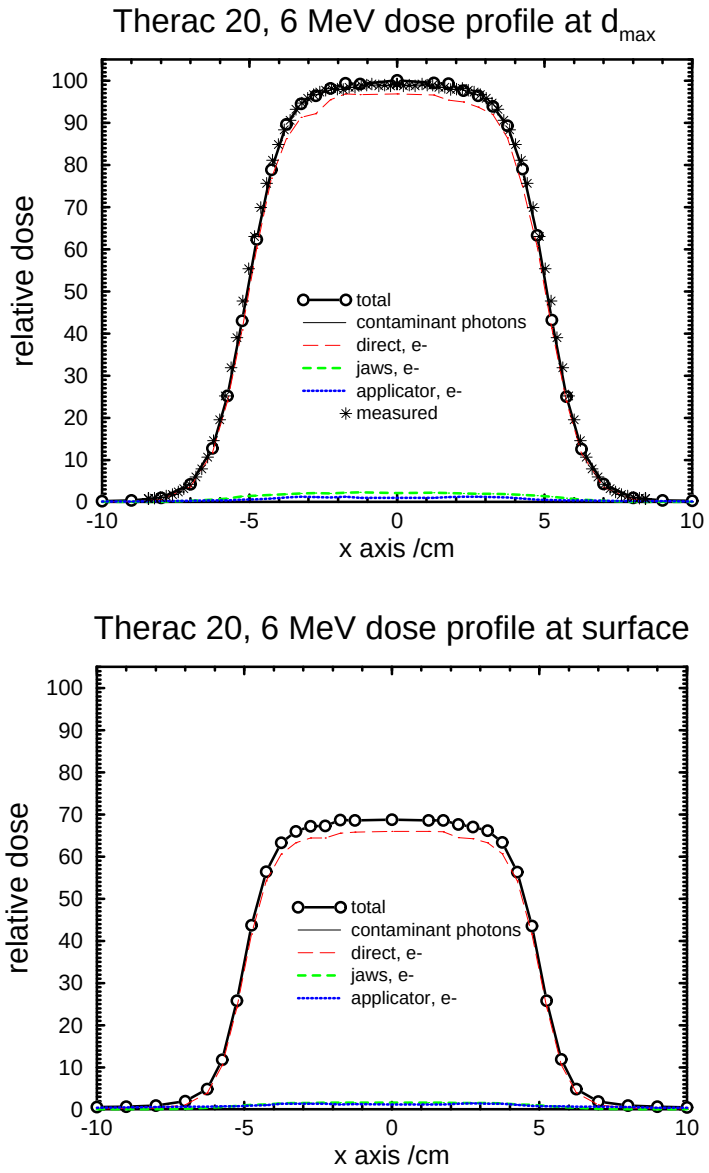

Figure 31: Calculated and measured dose profiles at d_{max} (upper) and at the phantom surface (lower) from various dose components in a 6 MeV beam from the AECL Therac 20.

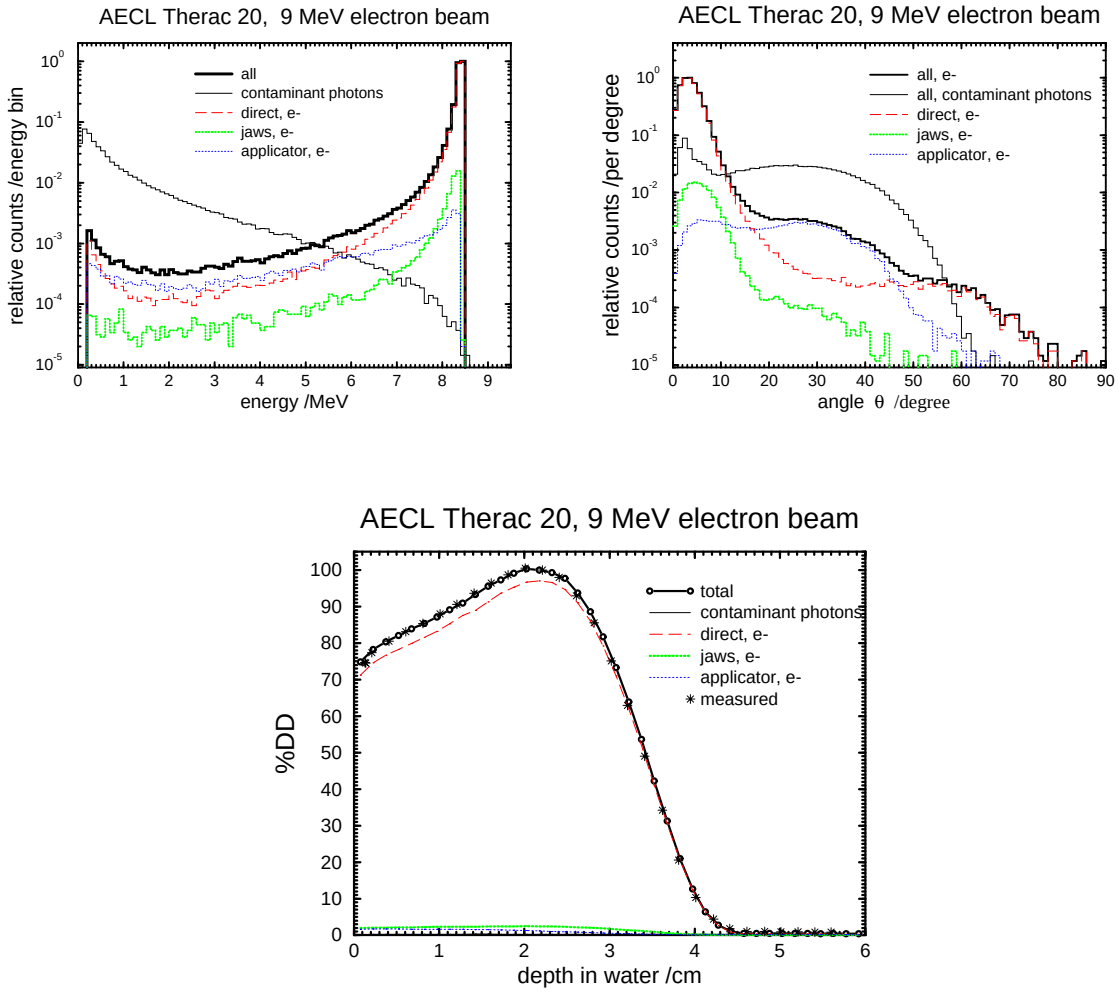

Figure 32: The energy spectra (upper left) and angular distributions (upper right) from various components at the phantom surface and inside the 10×10 cm^2 field of a 9 MeV electron beam from the AECL Therac 20. The normalization values are 8.95×10^5 and 3.42×10^5 for the spectra and the angular distributions respectively. The lower figure is a comparison between measured and calculated depth-dose curves along with dose components contributed from each beam defining component.

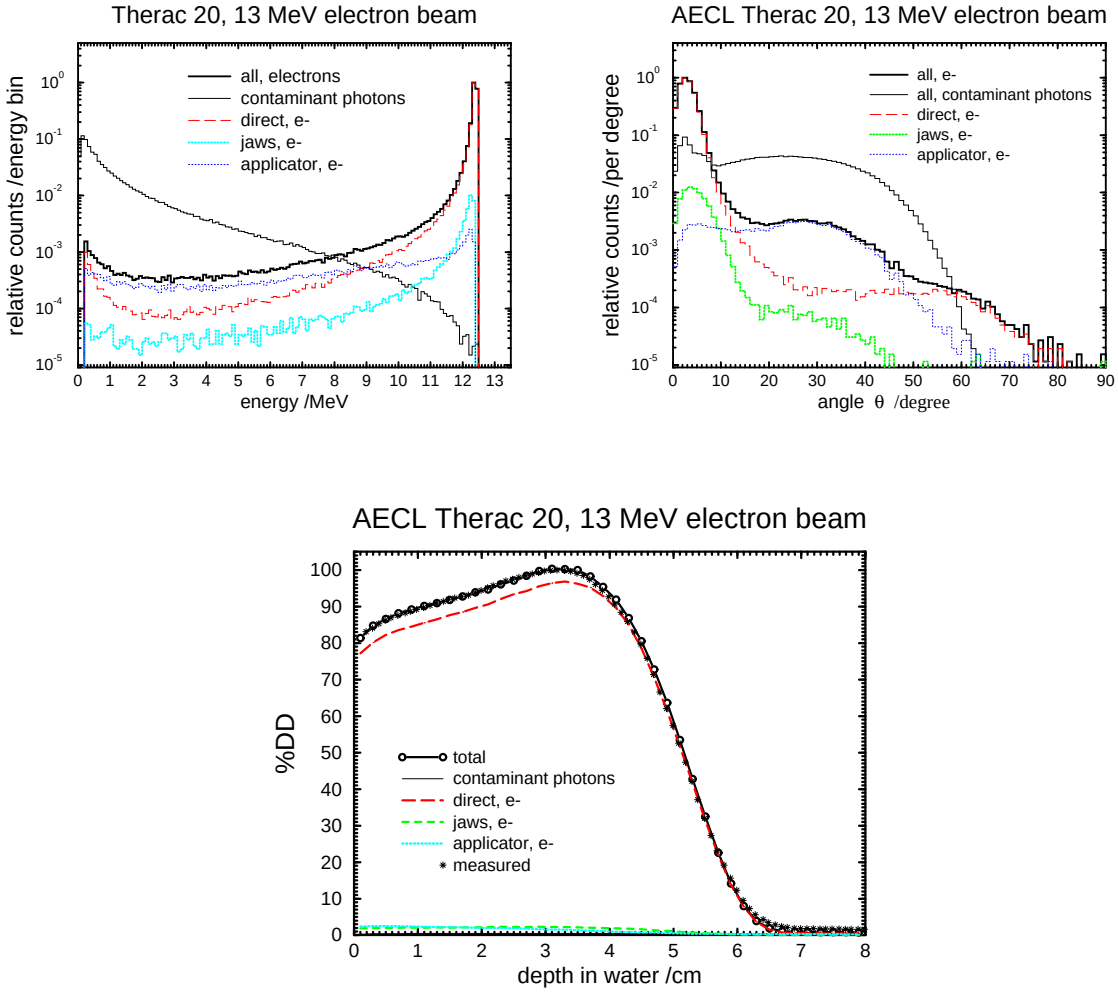

Figure 33: The energy spectra (upper left) and angular distributions (upper right) from various components at the phantom surface and inside the 10×10 cm^2 field of a 13 MeV electron beam from the AECL Therac 20. The normalization values are 4.71×10^5 and 2.61×10^5 for the spectra and the angular distributions respectively. The lower figure is a comparison between measured and calculated depth-dose curves along with dose components contributed from each beam defining component.

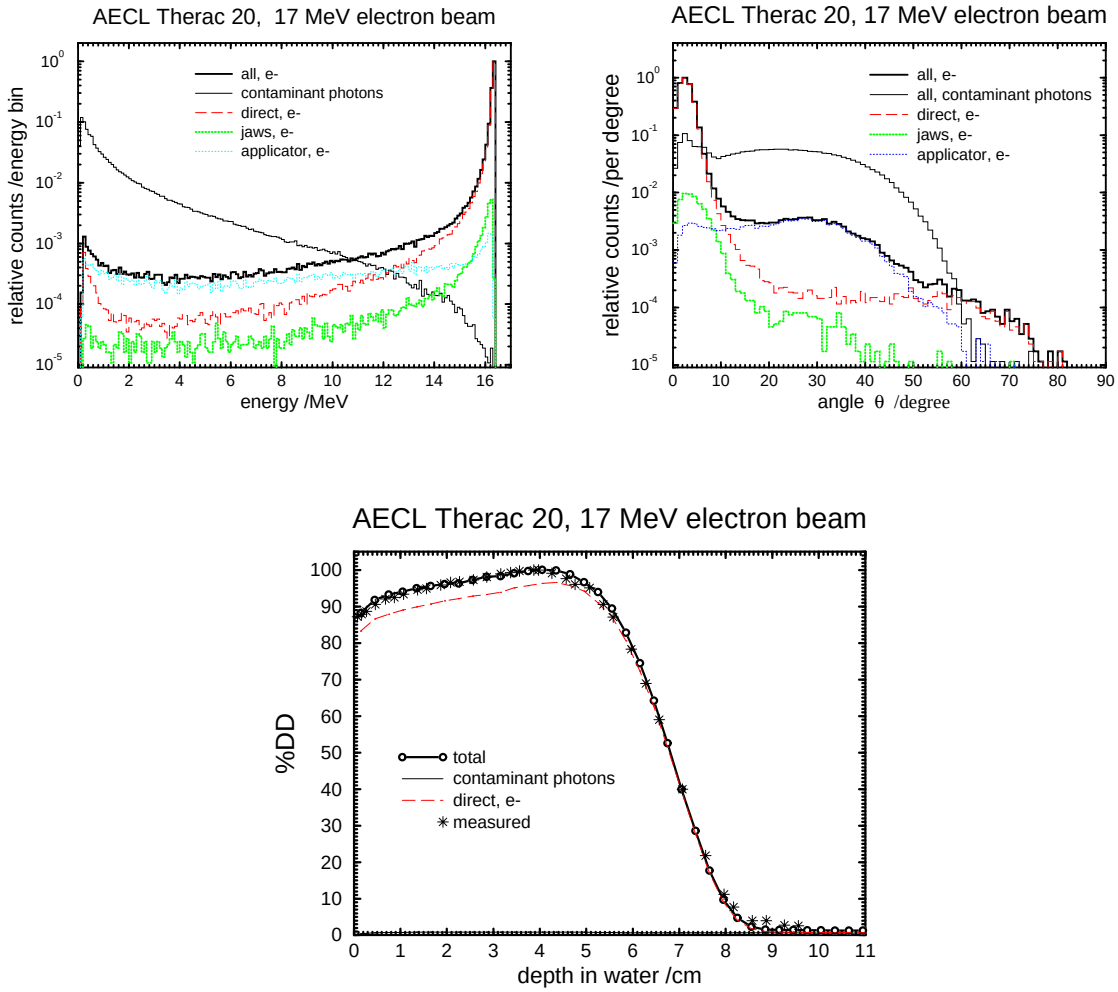

Figure 34: The energy spectra (upper left) and angular distributions (upper right) from various components at the phantom surface and inside the 10×10 cm^2 field of a 17 MeV electron beam from the AECL Therac 20. The normalization values are 4.02×10^5 and 1.74×10^5 for the spectra and the angular distributions respectively. The lower figure is a comparison between measured and calculated depth-dose curves along with dose components contributed from each beam defining component.

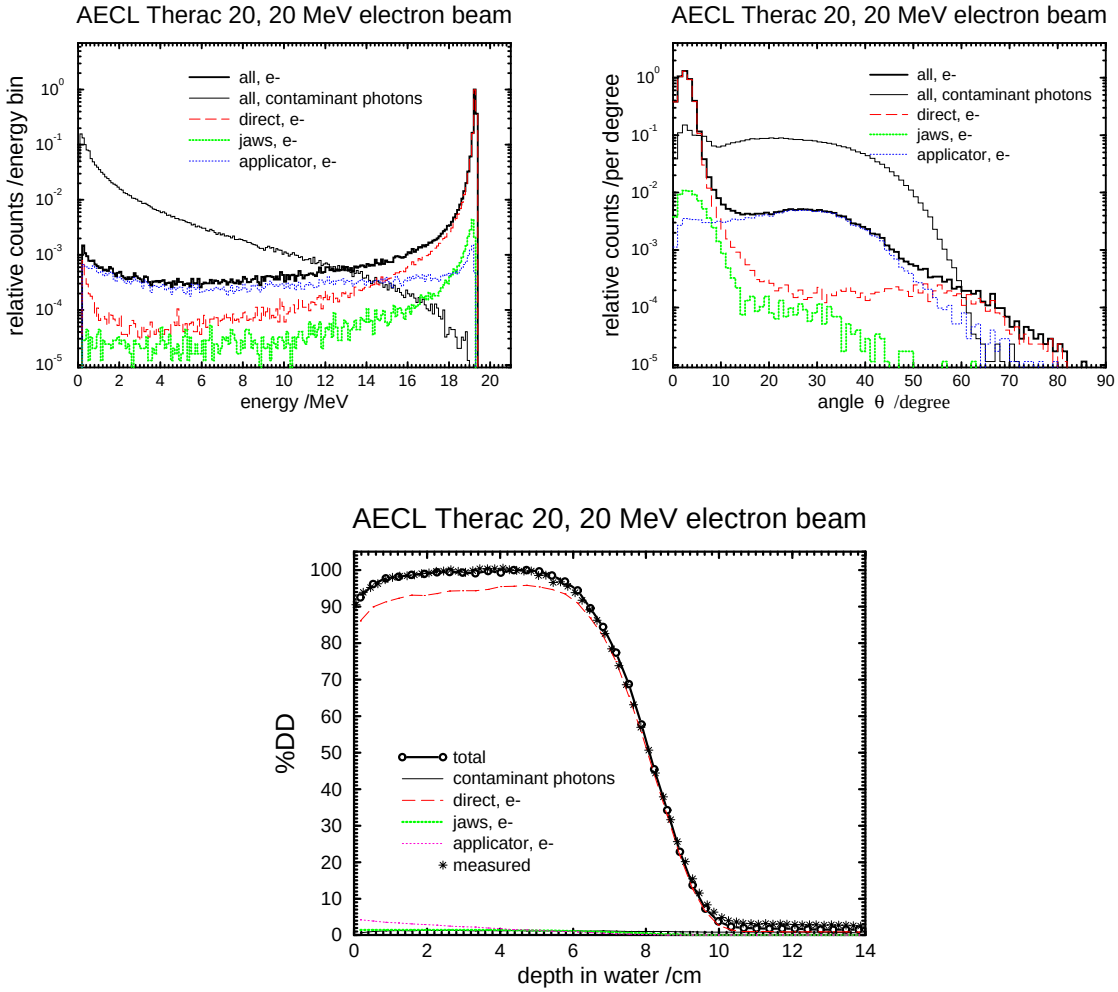

Figure 35: The energy spectra (upper left) and angular distributions (upper right) from various components at the phantom surface and inside the 10×10 cm^2 field of a 20 MeV electron beam from the AECL Therac 20. The normalization values are 2.76×10^5 and 2.27×10^5 for the spectra and the angular distributions respectively. The lower figure is a comparison between measured and calculated depth-dose curves along with dose components contributed from each beam defining component.

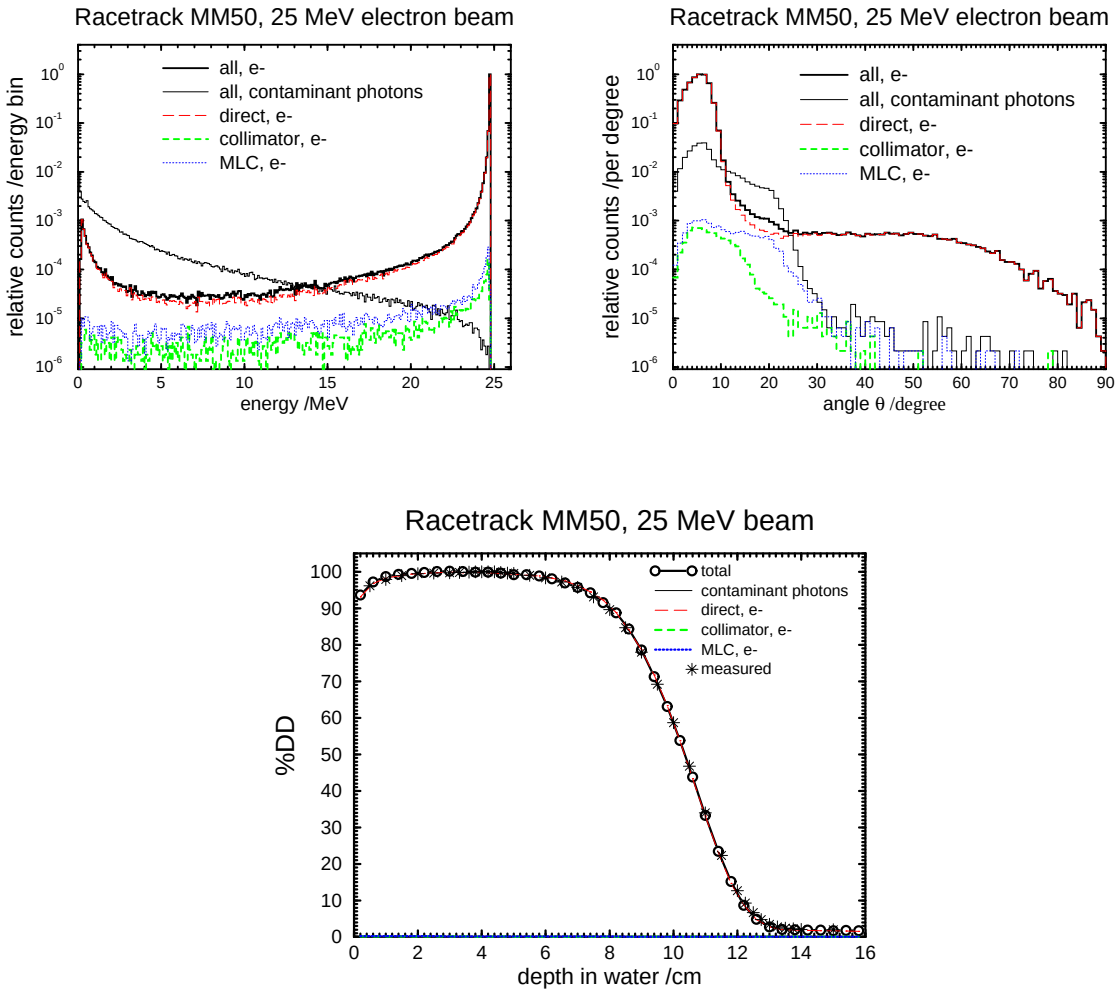

Figure 36: The energy spectra (upper left) and angular distributions (upper right) from various components at the phantom surface and inside the 25×25 cm^2 field of a 25 MeV electron beam from the Scanditronix Medical Microtron 50 at Memorial Sloan-Kettering Cancer Center. The normalization values are 2.26×10^5 and 4.68×10^5 for the spectra and the angular distributions respectively. The lower figure is a comparison between measured and calculated depth-dose curves along with dose components contributed from each beam defining component.

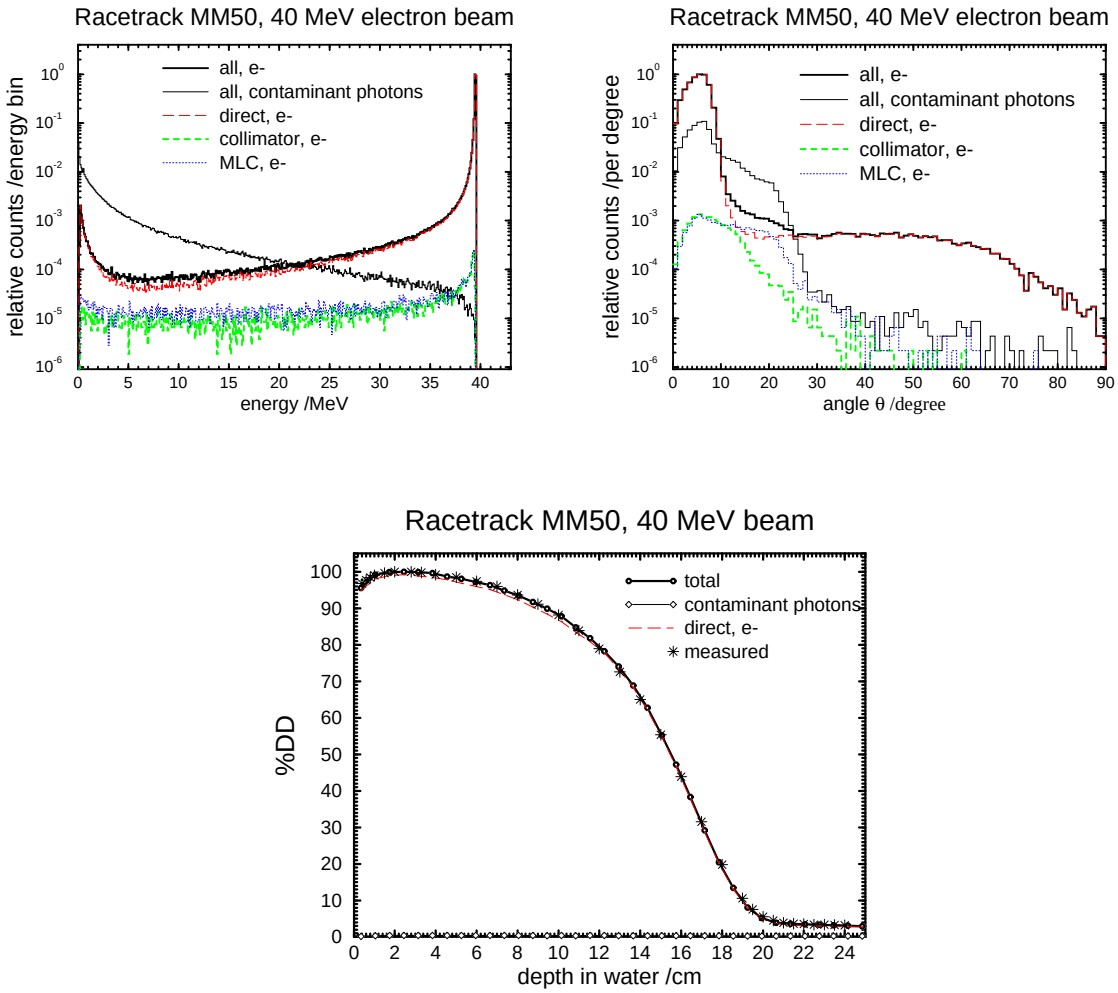

Figure 37: The energy spectra (upper left) and angular distributions (upper right) from various components at the phantom surface and inside the 25×25 cm^2 field of a 40 MeV electron beam from the Scanditronix Medical Microtron 50 at Memorial Sloan-Kettering Cancer Center. The normalization values are 1.23×10^5 and 4.62×10^5 for the spectra and the angular distributions respectively. The lower figure is a comparison between measured and calculated depth-dose curves along with dose components contributed from direct electrons and contaminant photons.

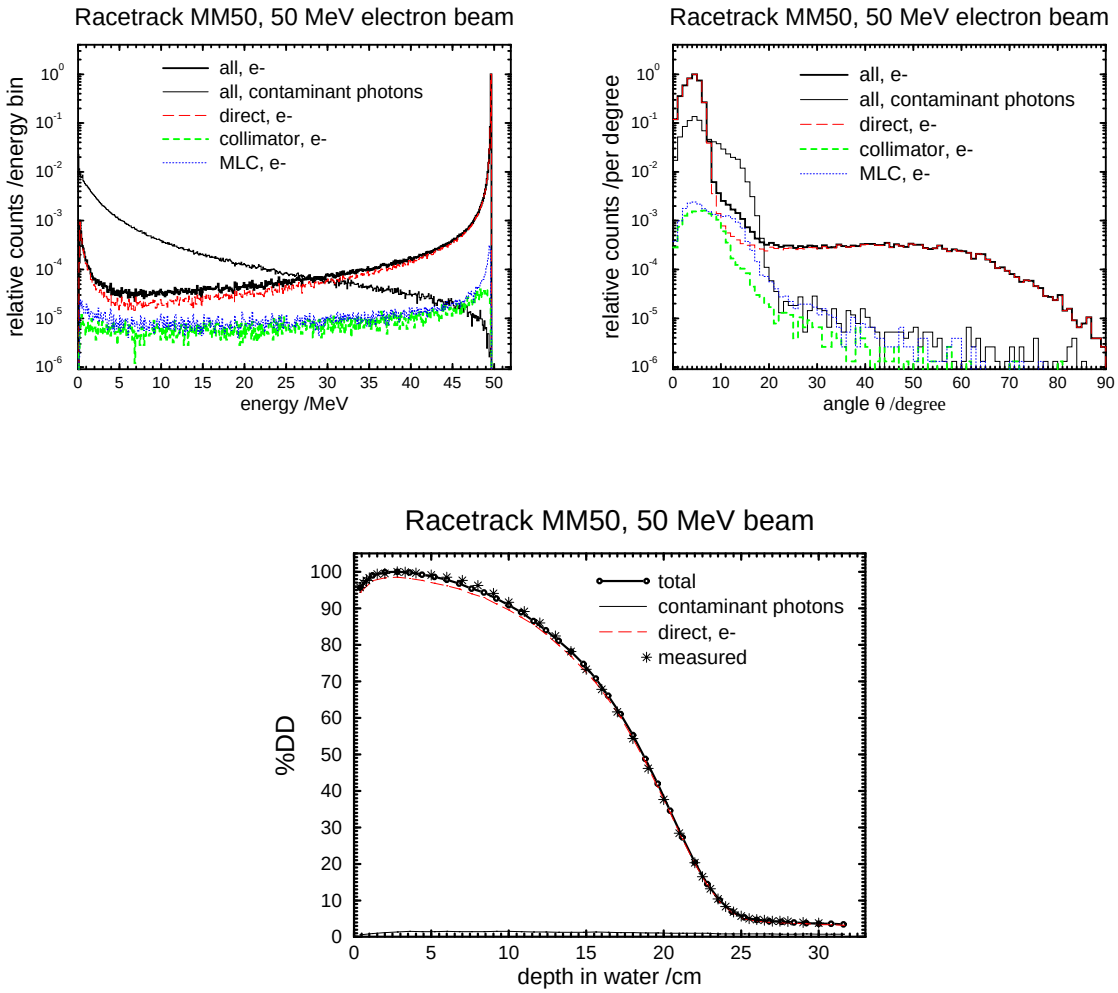

Figure 38: The energy spectra (upper left) and angular distributions (upper right) from various components at the phantom surface and inside the 20×20 cm^2 field of a 50 MeV electron beam from the Scanditronix Medical Microtron 50 at Memorial Sloan-Kettering Cancer Center. The normalization values are 1.39×10^5 and 7.68×10^4 for the spectra and the angular distributions respectively. The lower figure is a comparison between measured and calculated depth-dose curves along with dose components contributed from direct electrons and contaminant photons.

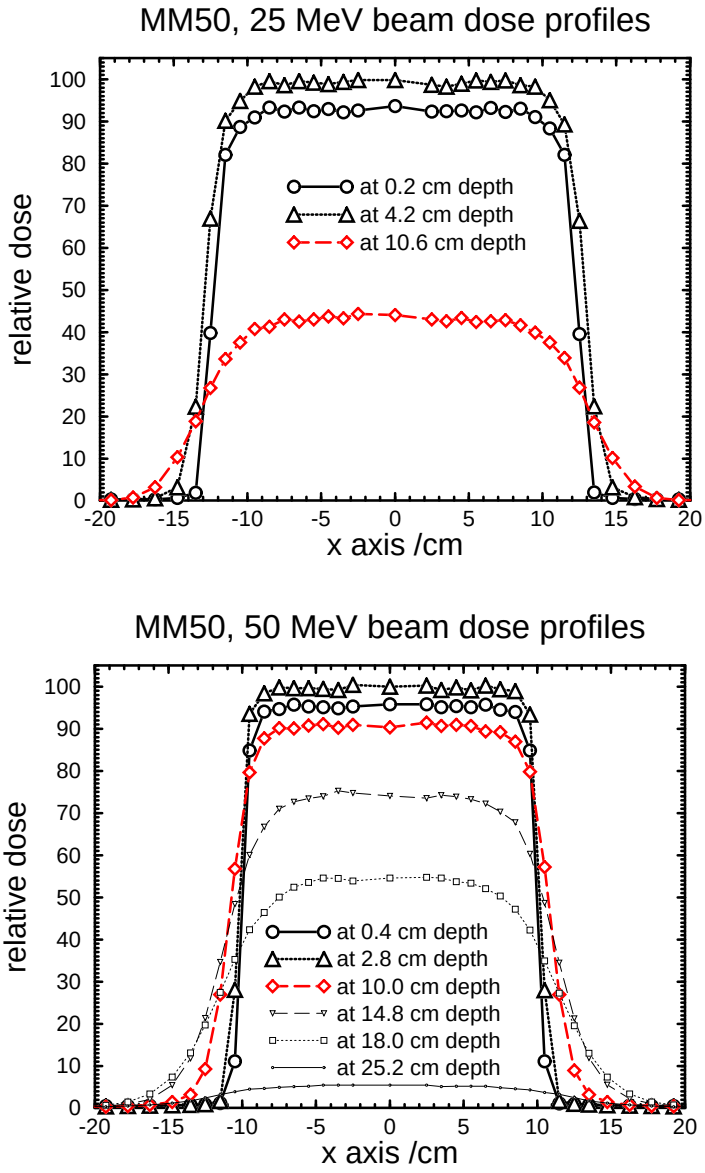

Figure 39: Calculated dose profiles at various depth in a water phantom for a 25 MeV (upper) and a 50 MeV (lower) beams from the Scanditronix Medical Microtron 50 at Memorial Sloan-Kettering Cancer Center.

References

[1] D.W.O. Rogers, B.A. Faddegon, G.X. Ding, C.-M. Ma, J. Wei and T.R. Mackie, "BEAM: A Monte Carlo code to simulate radiotherapy treatment units," Med. Phys. **22** (5) (1995).

[2] G.X. Ding, D.W.O. Rogers, and T.R. Mackie, "Electron beam spectra from different accelerators in radiotherapy," Med. Phys. **21** (abs) 1364 (1994).

[3] J.O. Deasy, "Electron energy and angular distributions in radiotherapy," PhD Thesis University of Kentucky (1992).

[4] A.F. Bielajew, and P.E. Weibe, "EGS-Windows - A Graphical Interface to EGS," NRCC Report: PIRS-0274 (1991).

[5] D.W.O. Rogers and A.F. Bielajew, "Monte Carlo techniques of electron and photon transport for radiation dosimetry," in "The Dosimetry of Ionizing Radiation",Vol III, eds. K.R. Kase, B.E. Bjarngard, and F.H. Attix, (Academic Press) 427 – 539 (1990).

[6] G.X. Ding, D.W.O. Rogers and T.R. Mackie, "Calculation of stopping-power ratios using realistic clinical electron beams," Med. Phys. **22**(5) (1995).

[7] A.F. Bielajew and D.W.O. Rogers, "PRESTA: The Parameter Reduced Electron-Step Transport Algorithm for Electron Monte Carlo Transport," Nuclear Instruments and Methods **B18** 165 – 181 (1987).

[8] G.X. Ding, D.W.O. Rogers and T.R. Mackie, "Mean energy, energy-range relationships and depth-scaling factors for clinical electron beams," submitted to Med. Phys. (April, 1995).

[9] C.K. Ross and K.R. Shortt, "Energy Calibration of the 90-B Beam Line of the IRS Linac," NRC Report Report PIRS-0021 (1985).

[10] G.X. Ding, D.W.O. Rogers, C.K. Ross, J.S. Wei, A.F. Bielajew, B.A.Faddegon, T.R. Mackie, P. Jursinic and J. Deasy, "Measured vs Monte Carlo calculated electron beam dose distributions," Med. Phys. **20** (abs) 933 (1993).

[11] A. Kassaee, M.D. Altschuler, S. Ayyalasomayajula and P. Bloch, "Influence of cone design on electron beam characteristics on clinical accelerators," Med. Phys. **21** 1671 – 1676 (1994).

[12] M. Udale, "A Monte Carlo investigation of surface doses for broad electron beams," Phys. Med. Biol. **33** 939 – 954 (1988).

[13] M. Udale-Smith, "A Monte Carlo Investigation of High Energy Electron Beams Used in Radiotherapy," PhD Thesis, Leeds University (1990).

[14] M. Udale, "Monte Carlo calculations of electron beam parameters for three Philips linear accelerators," Phys. Med. Biol. **37** 85 – 105 (1992).

[15] G.X. Ding, D.W.O. Rogers, J. Cygler and T.R. Mackie, "Electron fluence correction factors used in conversion of dose measured in plastic to dose in water," submitted to Med. Phys. (April, 1995).